THE UNIVERSITY OF MICHIGAN

Unclassified

2488-1-T

2488-1-T = RL-2054

RADAR CROSS-SECTION OF CONICAL BODIES OF REVOLUTION

by

K. M. Siegel

With the assistance of

H. Brysk, J. W. Crispin,

R. E. Kleinman, and

R. F. Goodrich.

GP #4
DECL 1960

This work was performed for the
Cornell Aeronautical Laboratory, Inc.
under C.A.L. Purchase Order No. CA-1704.9
31 October 1956

Unclassified

ERRATA SHEET
2488-1-T

Page No.		Corrections
8	Accoustic Graph - (10:1) Prolate Spheroid	(1) Vertical scale is incorrectly labeled 10^1 should be replaced by 10^0 10^0 should be replaced by 10^{-1} 10^{-1} should be replaced by 10^{-2} (2) The second maxima appears to be slightly less than 10^0, it should be slightly greater than 10^0. (3) The curvature shown on the graph should be reduced in the vicinity of the third maxima to show the amplitude is just above 1 at that maximum but less than the value at the second maximum.
17	line 6	The semi-axes should be given by a,a, $\frac{a}{\sqrt{1-\epsilon^2}}$ not a, a, $\frac{a}{1-\epsilon^2}$.
30	line 1	The word cross-section is misspelled.
33	line 6	$(kc)^2$ appears twice but should only appear once.
33	equations B.9 and B.10	The argument of the $\sec^2$ term should be α
46		In integral expressions for $\vec{n}_o \cdot \vec{f}$, the tan should be replaced by tan γ.
53		The Figure No. should be changed from D-8 to D-7.
69	equation at bottom of page	The decimal point is misplaced in the numerical coefficient, i.e. 0.33 should be replaced by .033.

TABLE OF CONTENTS

Unclas

ABSTRACT

From known exact results in acoustics and electromagnetic theory for the prolate spheroid, one predicts that the length of the resonance region depends on the length-to-width ratio of the scatterer. It is found that physical optics formulas previously used by us for thin cones are not applicable to large length-to-width ratio cones. New approximate formulas are derived for cones and cone-cylinder combinations. It is found that in the cases where the wavelength is large with respect to the dimensions of the object, for bodies of revolution with the incident Poynting vector on the axis of symmetry, the back scattering cross-section can be approximated roughly by $\frac{4}{\pi} k^4 V^2$, where k is $\frac{2\pi}{\lambda}$, and V is the volume. For all prolate spheroids, the rough formula given above yields results correct within 12 percent. For a flat body a correction factor is called for, and this is presented. It is found that for all spheroids this correction factor yields the exact Rayleigh result within 1 percent. New conclusions are drawn about the resonance region, but they are too complicated to summarize in this abstract.

The analysis reported here was done under several contracts. However, its applications to the CAL project PLATO became obvious, and as a result the analysis was pushed towards conclusions affecting the CAL study. The work of Brysk, Crispin, and Kleinman was performed under AF 04(645)-33, while the work of Goodrich was performed under Purchase Order L 265165-F31 with the Hughes Aircraft Company.

THE RADAR CROSS-SECTION OF CONICAL BODIES OF REVOLUTION

In examining the radar reflection characteristics of a perfectly conducting finite body of revolution it is convenient to distinguish between three wavelength regions:

(1) the Rayleigh region, where the wavelength of the radiation is large compared with all characteristic dimensions of the body;

(2) the physical optics region, where the wavelength of the radiation is small compared with almost all characteristic dimensions of the body; *

(3) the resonance region, intermediate between the other two.

In the first two regions good approximations to the cross-section can be obtained without recourse to the exact solution of the electromagnetic theory boundary value problem. This solution is unavailable for all finite bodies except the spheroid, in which case electronic computations are required. Such computations have been carried out in a very few cases. In the Rayleigh region, we develop from Rayleigh's results for spheroids a procedure for approximating the cross-sections of other bodies of revolution, and illustrate the method for several of the more common shapes. In the physical optics region, the cross-sections of a number of bodies of revolution have previously been given (Ref. 1); we present here several new results. In the resonance region, we indicate how a qualitative description of the cross-section can be obtained in the absence of a direct

* A noteworthy exception is a conical point.

solution by combining our knowledge of the cross-section in the other two regions with the results of certain physical arguments; in some cases the cross-section in the resonance region can thus be pretty well delineated.

Explicitly, we find for the Rayleigh region that the backscattering cross-section of an elongated body of revolution for incidence along the axis of symmetry is given by

$$\sigma = \frac{4}{\pi} k^4 V^2$$

where k is the wave number, and V the volume of the body. For bodies that cannot be considered elongated (along the axis of symmetry) a correction factor must be applied to the above expression to obtain more accuracy. We alter V to VF where

$$F = 1 + \frac{1}{\pi y} e^{-y}$$

and the elongation factor y is the ratio of the characteristic dimension along the axis of symmetry to the characteristic dimension perpendicular to the axis of symmetry. For geometrical configurations that allow this transformation, y is determined by contracting the body to a disc and requiring that it assume the correct cross-section in the limit; this is illustrated for several of the more common shapes. For scattering in other directions, the Rayleigh cross-section is obtained by approximating the body by the equivalent spheroid - i.e., replacing it by a spheroid with the same axis of symmetry, volume, and elongation factor. The Rayleigh cross-section of a spheroid for slant incidence is derived. Details will be found in Appendix A.

To determine radar cross-sections using physical optics, certain simplifying assumptions are made about the nature of the incident wave and the scattering body. One of these assumptions restricts the possible bodies to those whose normals vary continuously over the surface. In practice, however, failure to satisfy this requirement has proven to be no bar to successful application of the method. It is not the intent here to explain why the optics approximation can be successfully applied in a wider range of cases than is indicated by its derivation, but merely to present some heuristic criteria for determining the validity of the physical optics results, whether or not the continuity requirement is met, with particular emphasis on the finite cone.

Those bodies with point discontinuities or sharp edges that have been treated as scatterers using physical optics include cones (finite and semi-infinite), ogives, wedges, cylinders, and flat plates and discs. The semi-infinite cone and the thick ogive, considering just the tip result, are the most outstanding examples of the successful application of physical optics to bodies outside the purported range of validity. As for the other bodies, it was expected and has indeed been verified that in spite of the existence of a sharp edge, the physical optics approximation is a good one when the normal to the surface is parallel to the direction of incidence. This condition is nearly present for very thick cones.* Indeed, in the limit as the cone approaches a disc, the physical optics cone result approaches the physical optics disc result. Thus, at least for thick cones,

* The designations "thick" and "thin" are, of course, quite arbitrary. For the present, a cone half-angle of 15° will be taken to delimit "thick" and "thin" cones.

it is expected that the physical optics approximation will yield good results. In the case of thin cones viewed nose-on, however, the situation is one where the incident and surface normal directions are considerably separated. This is an example in which one should improve upon the results predicted by physical optics. The physical optics result for the finite cone, generalized to include incidence at small angles off nose-on, is derived in Appendix B. In view of the comments above, specifying that the wavelength be small is not sufficient to assure the validity of the optics approximation and, therefore, these results should be used with caution.

Reasoning from known exact solutions one can predict where one would expect pitfalls in using physical optics. If one considers the source and observer near one of the plane faces of a wedge but far from the wedge edge one finds the return from the wedge edge is considerable. This is not predicted by physical optics! One then realizes that as finite cones become longer and thinner, the same pitfall can be expected to exhibit itself. This, in fact, occurs, as can be observed from all known experimental results. We now present a method which enables one to obtain good theoretical estimates of the cross-sections of cones for such a situation. The advantage of this method lies in that it is a more accurate representation of the physical situation and is readily extended into the small wavelength or "optics" side of the resonance region. It is expected that due to the behavior of surface currents in the neighborhood of corners and edges, the dominant contribution to the cross-section of thin cones at nose-on aspects should come from the ring singularity at the base. (The tip contribution

is known to be small from the exact solution of the semi-infinite cone problem.) Thus an adequate treatment of the base of the cone should provide a good approximation to the behavior of the entire cone. In essence, the procedure is to approximate the base by an array of straight segments, find the scattered field due to each segment (neglecting end effects), and integrate around the base. (This is similar to defining a circle as a polygon whose number of sides increases without limit.) This has been done by treating each segment as a thin wire (Appendix C) and also by treating each segment as a wedge (Appendix D). The small wavelength restriction still must be met.

For the resonance region (aside from the very few cases in which the exact solutions of the Maxwell equations and the boundary conditions are available), we achieve a qualitative -- in some cases near-quantitative -- description by extending the results obtained in the Rayleigh and physical optics regionsby means of some assumptions based on experience as to the behavior of the cross-section as the resonance region is approached from either end, and also from the general ideas about, and models of, the resonance region proper. The extent of the resonance region is determined by the range of wavelengths for which the wavelength is neither very large nor very small compared with all the characteristic dimensions of the body. If the characteristic dimensions are comparable, the resonance region is small; if they differ considerably from each other, it may be large. The ratio of characteristic dimensions also determines the general character of

the variation of the cross-section with wavelength.* It is convenient to use the concept of a major maximum - defined as a maximum whose amplitude equals or exceeds that of the first maximum on the Rayleigh side. The first maximum on the Rayleigh side is thus always a major maximum. The cross-section of an elongated body can be expected to have several major maxima, and thus to be difficult to approximate; the cross-section of a sufficiently flatter body should have only one, and it should be possible to bound it fairly narrowly. For instance (see Fig. 1), the exact theory solution for the 10:1 prolate spheroid shows several major maxima, while the sphere and the disc have only one. There is then some critical spheroid whose dimensions are such that all spheroids with greater $\frac{a}{b}$ (ratio of semi-major to semi-minor axis) have more than one major maximum and all spheroids with smaller $\frac{a}{b}$ have only one major maximum. In acoustics the situation is reversed. The sphere curve has several major maxima while the 10:1 spheroid has only one (see Fig. 2). In this case, there will be a critical spheroid such that all spheroids with greater $\frac{a}{b}$ ratios will have only one major maximum and all spheroids with smaller $\frac{a}{b}$ ratios will have several major maxima.

On the Rayleigh side of the resonance region, the Rayleigh cross-section is expected to provide a good upper bound to the actual cross-section, which falls gradually and monotonically below the Rayleigh result until the first maximum is reached. The initial behavior of this deviation can be obtained by Stevenson's method (Ref. 2) (an expansion of the Maxwell

* In this discussion, we assume that the radar cross-section divided by either the geometric optics cross-section or the physical optics result is plotted as a function of kd where $k=\frac{2\pi}{\lambda}$ and d is some dimension of the scatterer.

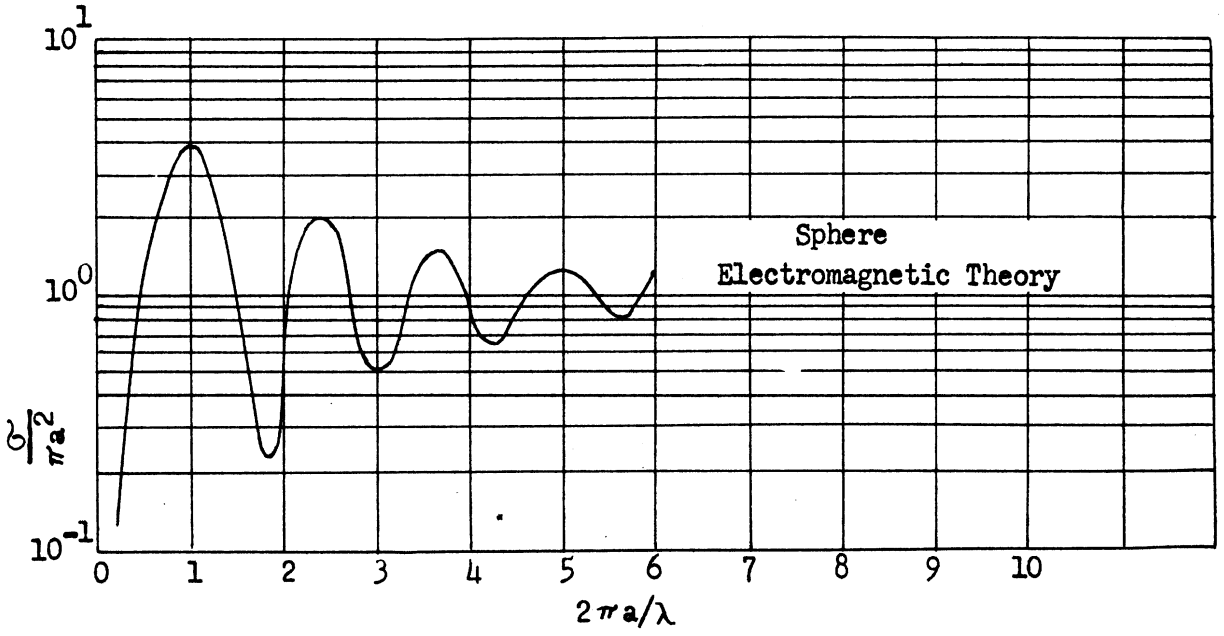

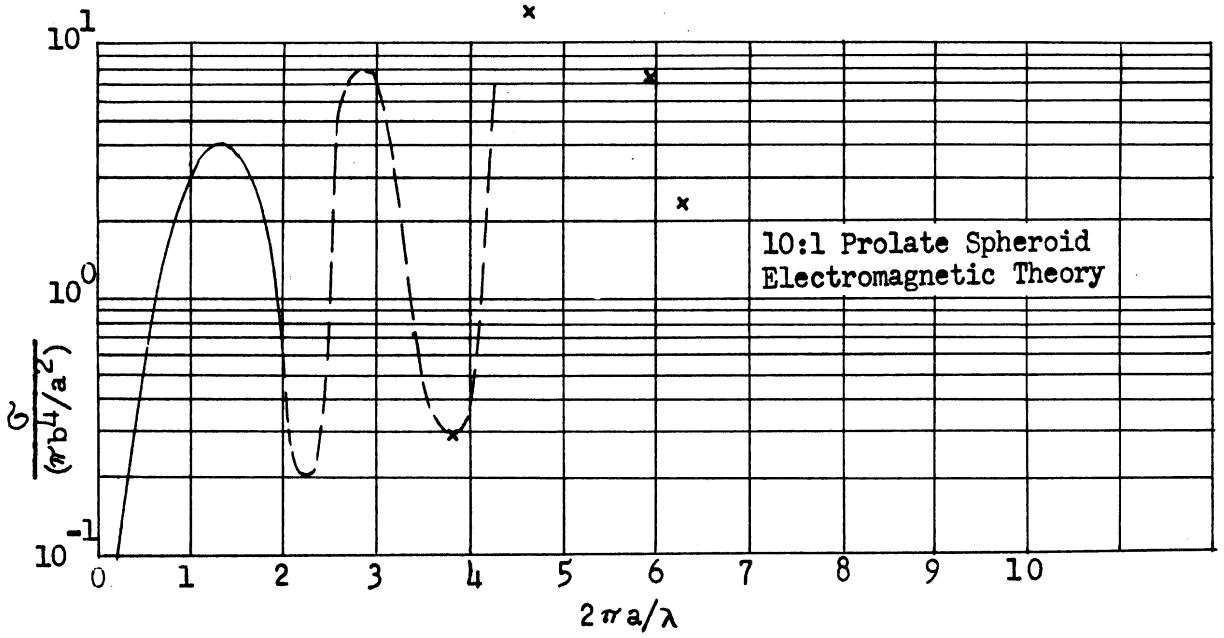

FIG 1: CROSS-SECTIONS OF THE SPHERE AND THE 10:1 PROLATE SPHEROID (ELECTROMAGNETIC THEORY)

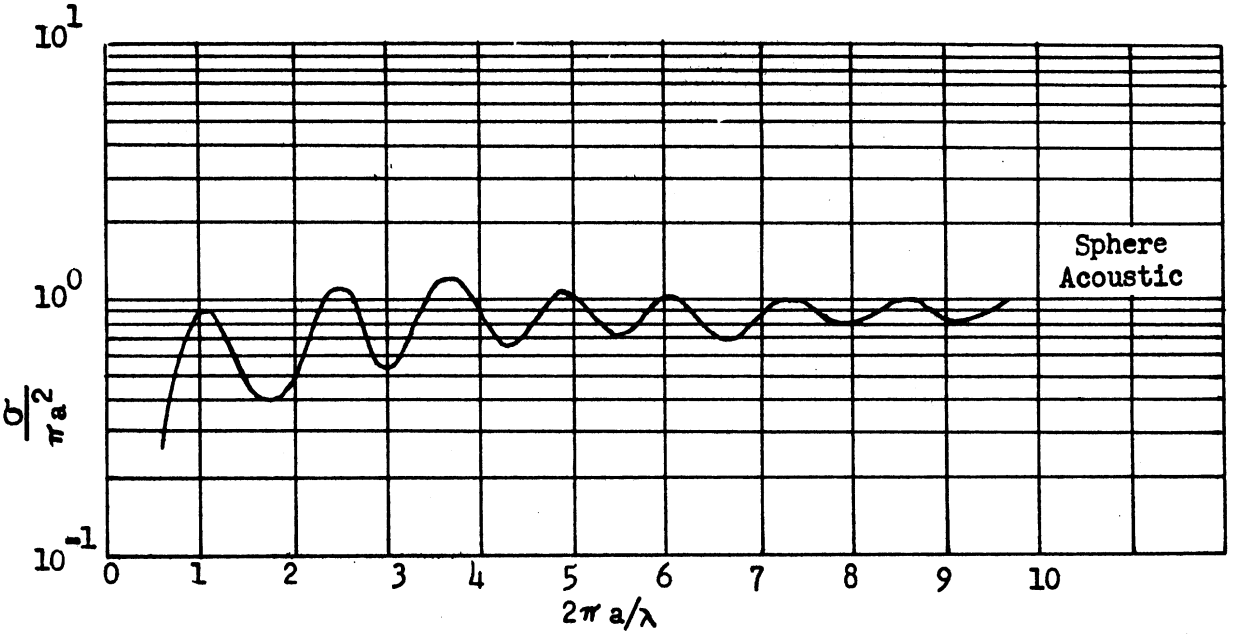

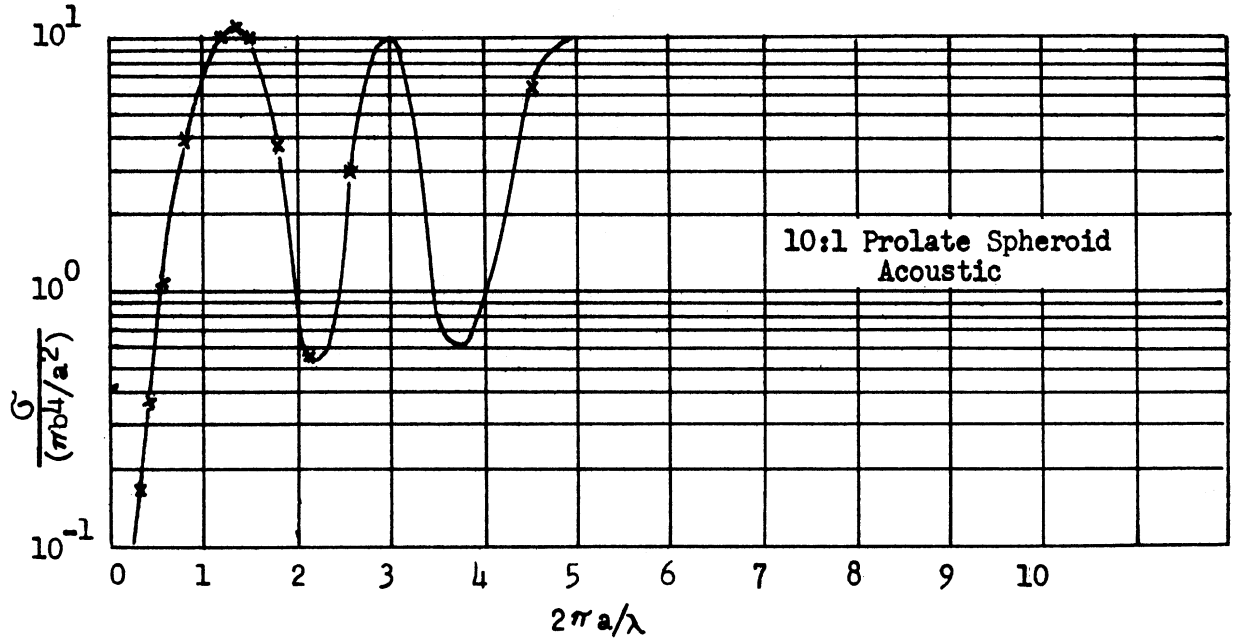

FIG 2: CROSS-SECTIONS OF THE SPHERE AND THE 10:1 PROLATE SPHEROID (ACOUSTIC THEORY)

equations in a power series in k, and solution of the resultant coupled equations for the coefficients) but this approach fails before the first maximum is reached. On the Rayleigh side of the resonance region, the cross-section is expected to depend on the major large linear characteristic dimensions of the body and not upon fine details of structure; this is in contrast to the dependence in the Rayleigh region where the dependence is on the volume of the body. A thin elongated body will behave like an antenna , i.e., its cross-section will have maxima whenever its length is equal to an integral number of half-wavelengths.

Assuming that the base is still the dominant feature of a thin finite cone as the resonance region is entered from the physical optics side, the resonance maximum of the ring singularity would approximate, in both position and amplitude, the last large maximum of the cone. Since in any physically realizable situation, the edge of the base of a cone will have a non-zero radius of curvature, b, ($b \ll \lambda$), the only difference between it and a wire loop (wire radius $\ll \lambda$) relative to incident electromagnetic energy is that currents can exist "inside" the loop but not "inside" the base of the cone.

When one looks at the axially symmetric cross-section of a ring as a function of wavelength one finds that there are no minima. This, then, allows one to predict that the contribution of the inner edge is negligible in comparison to the outer edge when the wavelength is equal to the order of the loop radius but greater than the wire radius. (If there were non-negligible contributions from both the outer and inner edges, then at some wavelengths they would add in phase and at some wavelengths they would add out of phase. But there are no noticeable minima in this region!)

Thus the cross-section of a loop here looks like a Rayleigh side-type answer, depending only on the loop radius but not on the wire radius. This, then, gives added justification for using an analogy between the conical base and the wire loop. Kouyoumjian's variational results (Ref. 4) for wire loops in the resonance region, can then be utilized. His results (as a function of wire radius and loop radius) indicate that the resonant peak is fairly insensitive to changes in wire radius but that as the wavelength decreases the wire radius becomes important. In the region of small wavelengths, the wire loop result can be used to furnish an upper bound on the cone result, since bounding the loop result will, in general, bound the cone result. (The small wavelength wire loop result is derived in Appendix C.)

There is another cone result in the small wavelength region that is obtained by treating the base of the cone, locally, as a wedge. Using physical optics to compute the fields due to the local wedges, and integrating, one obtains precisely the usual physical optics cone result (see Appendix D). Thus, even though physical optics is of dubious applicability, the two physical optics approximations yield consistent results. The wedge-type approximation is then carried out using for the scattered fields expressions generally more exact than physical optics. The resulting wedge-type cone answer is meant to apply only to thin cones and does not compete with the physical optics approximation for thick cones. This result, like the physical optics result, is independent of both polarization and wavelength; however, the two answers differ considerably for

thin cones, as we expected. Since Kouyoumjian has computed the wire loop cross-section in the resonance region, numerical values are available to match the "wedge" result for thin cones in the small wavelength region with the wire loop result in the resonance region. This yields an estimate of the section from the last large maximum out to the zero wavelength limit.

Consolidating all these considerations, we obtain an approximate description of the cross-section of the finite cone, covering the complete range of wavelengths for nose-on incidence. In the Rayleigh region, the cross-section is given by

$$\sigma = \frac{4}{9}\pi h^2 (kr)^4 \left(1 + \frac{1}{\pi h/4r} e^{-(h/4r)} \right)^2 ,$$

h = height, and
r = radius of base.

For a thin cone, the second term is negligible. In the resonance region, a thick cone should behave like a disc, which has a single major maximum. A thin cone can be expected to have more than one major maximum. The last large maximum on the optics side will be given by the wire loop. For all cones, subsidiary maxima may occur on the optics side of the wire loop (or disc) maximum.

In the optics region the cross-section for a thick cone is

$$\sigma = \frac{\pi \tan^4 \alpha}{k^2} \left| \frac{1}{2} + ikh - \frac{e^{2ikh}}{2} \right|^2 , \quad \alpha = \frac{1}{2} \text{ cone angle},$$

which for λ very small in respect to both r and h becomes

$$\sigma = \pi r^2 \tan^2 \alpha .$$

The cross-section for a thin cone is

$$\sigma = \frac{\pi^3 r^2}{\left(\frac{3\pi}{4} + \frac{\alpha}{2}\right)^2} \cot^2\left(\frac{\pi^2}{3\pi + 2\alpha}\right)$$

APPENDIX A

RAYLEIGH CROSS-SECTION OF BODIES OF REVOLUTION

Rayleigh scattering (Ref. 5) describes the scattering of electromagnetic radiation by a body whose dimensions are much smaller than the wavelength of the radiation. Thus the Rayleigh limit describes the scattered field due to an incident plane wave approximated at a large distance from the body by the field of radiating electric and magnetic dipoles located at the scatterer (the magnetic dipole contribution is comparable to that of the electric dipole only for a perfect conductor). To evaluate the electric (magnetic) dipole moment, the static electric (magnetic) field on the body due to a constant parallel incident field must be known. In other words, the electrodynamic boundary-value problem has been reduced to a corresponding static problem.

Although the solution of the Laplace Equation is in principle simpler than the solution of the Maxwell Equations, there are very few geometrical cases for which even the former is manageable. The question, therefore, arises whether any approximate information can be obtained as to the Rayleigh cross-section when a solution of the Laplace Equation is not available. That this should be possible is heuristically plausible. When the wavelength is much longer than the dimensions of a body, one cannot discern details of the structure of the body - the observed effect depends more on the size of the body than on its shape. Thus, knowledge of the size of the body, modified by a rough indication of shape, should suffice

for a good approximation to the Rayleigh cross-section. It is the purpose of the present discussion to explore this possibility.

For simplicity, consider the scatterer to be a body of revolution, and examine backscattering of a plane wave incident along the axis of symmetry. (Thus, the direction of incidence will be denoted by z, the incident electric vector direction by x, and the length of the body along the symmetry axis by L.) The electric dipole moment $\vec{p}$ is given by

$$\vec{p} = \int_S \omega \vec{r}\, dS \tag{A.1}$$

where ω is the charge density, $\vec{r}$ the position vector, and S is the surface of the body. The boundary condition yields

$$\omega = \epsilon \vec{E} \cdot \hat{n} = \epsilon E \tag{A.2}$$

where ϵ = dielectric constant, $\hat{n}$ = outward normal to the surface, and $\vec{E}$ = electric field strength.

Using cylindrical coordinates,

$$dS = \rho\, d\phi\, dz \tag{A.3}$$

where ρ is a function of z but not of ϕ, so that

$$\vec{p} = \epsilon \int_0^L \rho \int_0^{2\pi} E \vec{r}\, d\phi dz \quad . \tag{A.4}$$

From uniqueness and symmetry considerations, we can write

$$E = \sum_{n=0}^{\infty} a_n(z) \cos n\phi \quad . \tag{A.5}$$

Then $p_y = 0$, as it should, p_z does not concern us as it cannot contribute to the radiation (being along the direction of propagation), and

$$p_x = \epsilon \int_0^L dz \rho^2 \int_0^{2\pi} d\phi \cos\phi \sum_{n=0}^{\infty} a_n(z) \cos n\phi \tag{A.6}$$

$$= \epsilon \int_0^L dz \ \pi\rho^2 \ a_1(z) \quad .$$

Apart from the factor $a_1(z)$, the integral is just the volume of the body, V. In fact, the whole determination of the electric dipole moment resolves itself into the determination of the factor $a(z)$ in

$$E = a(z) \cos\phi \tag{A.7}$$

since the other terms in the series do not contribute. If the body is elongated along the axis of symmetry (i.e., if $L \gg \rho$), $a(z)$ will be a slowly varying function of z and can be removed from the integral and replaced by a mean value (or actually by an estimate of its value). To estimate $a(z)$, we resort to an analogy with reflection from a plane. In the latter case, the amplitude of the total field is twice that of the incident field. Thus we choose $a = 2E_0$ (phase differences in the incident field at various points on the body can be neglected) to obtain

$$\vec{p} = \hat{x} \ 2\epsilon E_0 V \quad . \tag{A.8}$$

The far-zone electric field due to the electric dipole is (Ref. 6)

$$\vec{E} = -\frac{k^2}{4\pi\epsilon}\ \hat{z} \times (\hat{z} \times \hat{p})\ \frac{e^{i(kR - \omega t)}}{R} \quad . \tag{A.9}$$

For a conductor, analogous treatment of the magnetic dipole yields an equal contribution in phase. Altogether, we have in the far-zone

$$\vec{E} = \hat{x}\ \frac{k^2}{\pi}\ E_o\ V\ \frac{e^{i(kR - \omega t)}}{R} \quad . \tag{A.10}$$

The cross-section is given by

$$\sigma = 4\pi R^2 \left|\frac{\vec{E}}{\vec{E}_o}\right|^2 = \frac{4}{\pi}\ k^4\ V^2 \quad . \tag{A.11}$$

This, then, is the value of the cross-section to be expected for an elongated body of revolution.* As the flatness of the scatterer increases, the approximation is expected to get worse, in fact an infinitely flat body (infinite radii of curvature) has a non-zero cross-section.

Let us now compare this pseudo-derivation with the exact answer for the special case we do know, the spheroid (Ref. 5). Let us define for convenience the quantity

$$F = \frac{\pi R\ |\vec{E}|}{k^2\ E_o V} \quad . \tag{A.13}$$

* It should be noted that for the acoustic case the treatment would be equivalent except that instead of the two components (electric and magnetic) there would be only one, and thus the cross-section would be

$$\sigma = \frac{1}{\pi}\ k^4\ V^2 \quad . \tag{A.12}$$

$F = 1$ yields the magnitude of $\vec{E}$ given by Equation A.10. Modifying Rayleigh's notation slightly,

$$F = \frac{1}{2}\left(\frac{1}{L} + \frac{1}{2-L}\right) = \frac{1}{L(2-L)} \qquad (A.14)$$

where, for a prolate spheroid, (Ref. 5),

$$L = \left(\frac{1}{e^2} - \frac{1-e^2}{2e^3} \log \frac{1+e}{1-e}\right) \qquad (A.15)$$

where e = eccentricity -- i.e., the semi-axes are a, a, $\frac{a}{1-e^2}$.

For an elongated spheroid ($e \to 1$), $L \to 1$ and $F \to 1$, checking the approximation.

Next, let us inquire into the shape correction by first examining its form for the spheroid. We already know the prolate result; for the oblate spheroid,

$$L = \left(\frac{\sqrt{1-e^2}}{e^3} \sin^{-1} e - \frac{1-e^2}{e^2}\right), \text{ (Ref. 5)} \qquad (A.16)$$

where the semi-axes are now a, a, $a\sqrt{1-e^2}$. As these expressions are quite complicated, it is profitable to examine their limiting values.

Consider a sphere ($e = o$): From (A.15)

$$\log \frac{1+e}{1-e} = 2\left(e + \frac{1}{3}e^3 + \ldots\right) \qquad (A.17)$$

$$L \approx \frac{1}{e^2}\left[1-(1-e^2)\left(1+\frac{1}{3}e^2\right)\right] \approx \frac{1}{e^2}\left[1-1+e^2-\frac{1}{3}e^2\right] = \frac{2}{3} \qquad (A.18)$$

$$F \approx \left(\frac{2}{3}\left(2-\frac{2}{3}\right)\right)^{-1} = \left(\frac{2}{3}\cdot\frac{4}{3}\right)^{-1} = \frac{9}{8} \quad . \qquad (A.19)$$

It is easily demonstrated that F is monotone decreasing as we progress from a sphere to an elongated prolate spheroid. Hence, it ranges from $\frac{9}{8}$ to 1 -- very nearly constant, of the form 1 + decaying term.

Examine the disc limit (e→1 for oblate spheroid):

Let

$$e = \sin x \quad . \qquad (A.20)$$

Then $L = \cos x \csc^2 x (x \csc x - \cos x)$. (A.21)

Let

$$y = \frac{\pi}{2} - x \quad . \qquad (A.22)$$

Then $L = \sin y \sec^2 y \left[\left(\frac{\pi}{2} - y\right) \sec y - \sin y\right]$. (A.23)

Expand near y = 0 (equivalent to e→1):

$$L \approx y\left[\left(\frac{\pi}{2} - y\right) - y\right] = \frac{\pi y}{2} - 2y^2 = \frac{\pi}{2} y \left(1-\frac{4}{\pi} y\right) \qquad (A.24)$$

$$F = \frac{1}{L(2-L)} \approx \frac{1}{\frac{\pi}{2} y\left(1-\frac{4}{\pi} y\right)\left(2-\frac{\pi}{2} y\right)} \approx \frac{1}{\pi y}\left(1+\frac{4}{\pi} y + \frac{\pi}{4} y\right) \quad . \qquad (A.25)$$

For small y, $y \approx \sqrt{1-e^2}$; if we call the semi-axes a, a, b, then $y = \frac{b}{a}$.

Combine the information about F. In the oblate case, F is again monotone, increasing toward the disc limit. The prolate spheroid discussion indicates that we should split off from F a unity term, and that the remaining term should decay as $y = \frac{b}{a} \to \infty$. Thus,

$$F \approx 1 + \frac{1}{\pi y}\left[1 + \left(\frac{4}{\pi} + \frac{\pi}{4} - \pi\right) y\right] \approx 1 + \frac{1}{\pi y}(1 - y) \approx 1 + \frac{1}{\pi y} e^{-y} . \tag{A.26}$$

We postulate, then, that for all spheroids (with semi-axes a, a, b), the shape correction factor is approximately

$$F = 1 + \frac{1}{\pi y} e^{-y} \tag{A.26}$$

where $y = \frac{b}{a}$. Numerical comparison indicates that the approximation is valid to within one percent. The Rayleigh cross-section of a spheroid for backscattering along the axis of symmetry is

$$\sigma = \frac{4}{\pi} k^4 v^2 \left(1 + \frac{1}{\pi y} e^{-y}\right)^2 \tag{A.27}$$

The cross-section of the spheroid depends on its volume and on a correction factor involving $y = \frac{b}{a}$. Except for very flat oblate spheroids, the shape correction factor can be neglected. Where it is not neglected, the shape correction factor is a simple function of y, which is a measure of the elongation.

The natural extension of the discussion is to postulate that for all bodies of revolution the Rayleigh cross-section for backscattering along the axis of symmetry can be expressed as

$$\sigma \sim \frac{4}{\pi} k^4 V^2 \left(1 + \frac{1}{\pi y} e^{-y}\right)^2 \qquad \text{(A.27)}$$

where y is a measure of the elongation (characteristic dimension along the axis of symmetry) / (characteristic dimension in the perpendicular direction). For elongated bodies, the term in y drops out and there is no ambiguity. For flattened bodies, the answer is sensitive to the choice of characteristic dimensions, but a good approximation should still be attainable. The ambiguity can be eliminated in a number of cases by imposing a restriction on the choice of characteristic dimensions: in the limit of extreme flattening, the cross-section must tend to the value for the appropriate disc.

Illustration I: Finite Cone

Consider a right circular cone of altitude h and radius of base r. As $h \to 0$, the cross-section of the cone must go into the cross-section of a disc of radius r --- i.e., we must have

$$VF = \frac{1}{3} \pi r^2 h \left(1 + \frac{1}{\pi y} e^{-y}\right) \to \frac{r^2 h}{3y} = \frac{4}{3} r^3 \quad . \qquad \text{(A.28)}$$

Thus, the appropriate ratio of characteristic dimensions to be used in Equation A.27 is

$$y = \frac{h}{4r} \quad . \qquad \text{(A.29)}$$

Hence, the cone has the same cross-section as a spheroid of equal volume whose semi-axes are (r, r, h/4).

Illustration II: Lens

Consider a symmetrical convex lens of radius of curvature R (the body of revolution obtained by rotating the shaded area in Figure A-1 about the η -axis). In the disc limit (d constant, $c \to 0$):

$$VF \to \frac{V}{\pi y} = \frac{4}{3} d^3 \qquad (A.30)$$

Hence, we take for the lens

$$y = \frac{3V}{4\pi d^3} = \frac{3V}{4\pi R^3 \sin^3 \theta} \quad . \qquad (A.31)$$

The volume of the lens is

$$V = \frac{2\pi}{3} R^3 (1-\cos\theta)(1-\cos\theta + \sin^2\theta) \quad . \qquad (A.32)$$

As $\theta \to \frac{\pi}{2}$ (sphere limit), we reproduce the previous spheroid result, as expected.

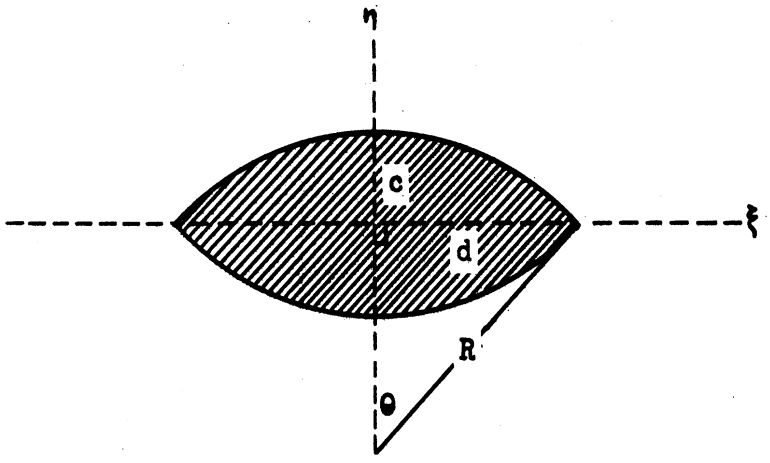

Figure A-1

Illustration III: Elliptic Ogive

Inasmuch as the circular ogive is more elongated than a sphere, the argument from the disc limit connot be applied to it directly.

Instead, we consider the elliptic ogive obtained by rotating the shaded area of Figure A-2 (a portion of an ellipse) about the η-axis (which is taken parallel to the minor axis). For this body, in the disc limit (d constant, $c \to 0$):

$$VF \to \frac{V}{\pi y} = \frac{4}{3} d^3 \quad . \tag{A.33}$$

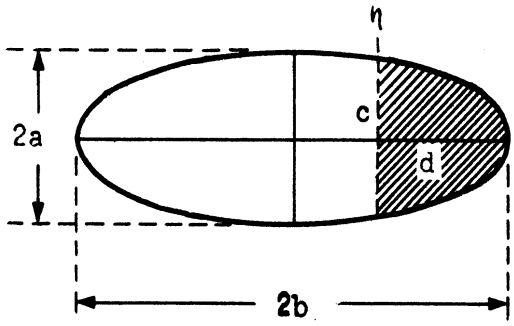

FIG A-2

From the equation for the ellipse,

$$\frac{c^2}{a^2} + \frac{(b-d)^2}{b^2} = 1, \tag{A.34}$$

which suggests use of the parameter θ:

$$\sin\theta = \frac{c}{a} \quad . \tag{A.35}$$

Then

$$y = \frac{3V}{4\pi d^3} = \frac{3V}{4\pi b^3 (1-\cos\theta)^3} \quad . \tag{A.36}$$

The volume of the elliptic ogive is

$$V = 2\pi ab^2 (\sin\theta - \theta\cos\theta - \tfrac{1}{3}\sin^3\theta) \tag{A.37}$$

As $\theta \to \frac{\pi}{2}$, we reproduce the previous spheroid result, as expected.

Special Case: Circular Ogive. To obtain the cross-section of the circular ogive, we now merely take the special case of the elliptic ogive with a = b. This leads to the body obtained by rotating the shaded area of Figure A-1 about the ξ - axis. Now

$$y = \frac{3}{2} \frac{\sin\theta - \theta\cos\theta - \frac{1}{3}\sin^3\theta}{(1-\cos\theta)^3} \quad . \tag{A.38}$$

Illustration IV: Spindle

Consider the body of revolution obtained by rotating the shaded area of Figure A-3 (bounded by a parabola and a straight line perpendicular to the axis of the parabola) about the η -axis. Using the disc limit exactly as before, we have

$$y = \frac{3V}{4\pi d^3} \tag{A.39}$$

where the volume is

$$V = \frac{16}{15} \pi cd^2 \tag{A.40}$$

so that

$$y = \frac{4}{5}\frac{c}{d} \quad . \tag{A.41}$$

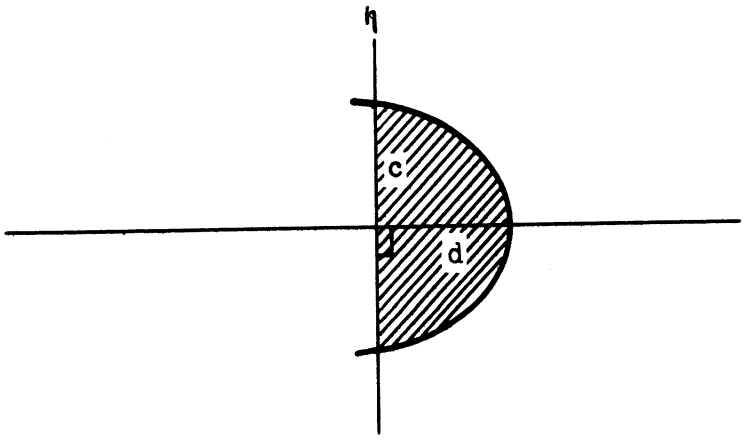

Figure A-3

Illustration V: Finite Cylinder

Consider a cylinder of radius r and height h. From the disc limit,

$$y = \frac{3V}{4\pi r^3} = \frac{3h}{4r} \qquad (A.42)$$

To evaluate the Rayleigh cross-section of a body of revolution (for any transmitter and receiver directions) the body is approximated by the equivalent spheroid. The equivalent spheroid is a spheroid with the same axis of symmetry, the same volume, and the same elongation factor, y, as the body. The simplification found for the backscattering along the symmetry axis provides a reasonable way to arrive at an elongation factor for many bodies.

Rayleigh quotes the far-zone scattered field for an ellipsoid for incidence along one principal axis (with coefficients evaluated for the special case of a spheroid)(Ref. 5). A simple permutation of coordinates

leads to the far-zone scattered field of a spheroid for incidence along any principal axis. The extension to slant incidence is not difficult, but requires a little more care. To take the polarization into account correctly, it is necessary to treat the contributions to the far-zone scattered field from the electric and magnetic incident fields separately. Using Rayleigh's results and appropriate rotations (with some slight changes of notation), the contributions to the far-zone scattered field from the various components of the incident field are:

(A.43)

$$\vec{E}_o = \hat{x}E_o \;:\; \vec{E} = -\frac{k^2 e^{i(kr-\omega t)}}{2\pi R}\frac{E_o V}{L_x}\left(-\frac{y^2+z^2}{R^2}, \frac{xy}{R^2}, \frac{xy}{R^2}\right)$$

$$\vec{E}_o = \hat{y}E_o \;:\; \vec{E} = -\frac{k^2 e^{i(kR-\omega t)}}{2\pi R}\frac{E_o V}{L_y}\left(\frac{xy}{R^2}, -\frac{x^2+z^2}{R^2}, \frac{yz}{R^2}\right)$$

$$\vec{E}_o = \hat{z}E_o \;:\; \vec{E} = -\frac{k^2 e^{i(kR-\omega t)}}{2\pi R}\frac{E_o V}{L_z}\left(\frac{xz}{R^2}, \frac{yz}{R^2}, -\frac{x^2+y^2}{R^2}\right)$$

$$\vec{H}_o = \hat{x}\epsilon cE_o \;:\; \vec{E} = -\frac{k^2 e^{i(kR-\omega t)}}{2\pi R}\frac{E_o V}{2-L_x}\left(0, -\frac{z}{R}, \frac{y}{R}\right)$$

$$\vec{H}_o = \hat{y}\epsilon cE_o \;:\; \vec{E} = -\frac{k^2 e^{i(kR-\omega t)}}{2\pi R}\frac{E_o V}{2-L_y}\left(\frac{z}{R}, 0, -\frac{x}{R}\right)$$

$$\vec{H}_o = \hat{z}\epsilon cE_o \;:\; \vec{E} = -\frac{k^2 e^{i(kR-\omega t)}}{2\pi R}\frac{E_o V}{2-L_z}\left(-\frac{y}{R}, \frac{x}{R}, 0\right)$$

If the z-axis is the axis of symmetry of the spheroid, we can take $\phi = 0$ without loss of generality. Then

$$x = R \sin\theta \qquad y = 0 \qquad z = R\cos\theta \tag{A.44}$$

The L's have been evaluated by Rayleigh. For our geometry,

$$L_x = L_y = L \tag{A.45}$$

where L is the quantity given by Equations A.15 and A.16. The expressions for L_z can be written in terms of those for L; the relation is

$$L_z = 2\,(1-L) \tag{A.46}$$

Consider now an incident plane wave travelling toward the origin in the direction θ_T. For arbitrary polarization, it can be expressed as a linear combination of the following two cases:

a) $\vec{E}_o$ in the plane defined by the Poynting vector and the axis of symmetry - i.e.,

$$\vec{E}_{oa} = (-\hat{x}\cos\theta_T + \hat{z}\sin\theta_T)E_o \quad , \quad \vec{H}_{oa} = \hat{y}\,\epsilon\, cE_o \quad . \tag{A.47a}$$

b) $\vec{E}_o$ perpendicular to this plane - i.e.

$$\vec{E}_{ob} = \hat{y}\,E_o \quad , \quad \vec{H}_{ob} = (\hat{x}\cos\theta_T - \hat{z}\sin\theta_T)\,\epsilon\, cE_o \quad . \tag{A.47b}$$

In each case, the far-zone scattered field is obtained by adding up the contributions (as given by Equation A.43) due to the components of the incident electric and magnetic fields that are present. In the direction of observation θ_R the results for the two cases are

$$\vec{E}_a = \frac{k^2 E_o V e^{i(kR-\omega t)}}{2\pi R}\left(\frac{1}{2-L} + \frac{\cos\theta_R\cos\theta_T}{L} + \frac{\sin\theta_R\sin\theta_T}{2-2L}\right) \qquad (A.48a)$$

$$x\left(-\cos\theta_R,\ 0\ ,\ \sin\theta_R\right)$$

and

$$\vec{E}_b = \frac{k^2 E_o V e^{i(kR-\omega t)}}{2\pi R}\left(\frac{1}{L} + \frac{\cos\theta_R\cos\theta_T}{2-L} + \frac{\sin\theta_R\sin\theta_T}{2L}\right)$$

$$x\left(0,\ 1,\ 0\right)\ . \qquad (A.48b)$$

If we again write

$$\sigma = \frac{4}{\pi}\ k^4\ V^2\ F^2 \qquad (A.49)$$

we now have

$$F_a = \frac{1}{2}\left(\frac{1}{2-L} + \frac{\cos\theta_R\cos\theta_T}{L} + \frac{\sin\theta_R\sin\theta_T}{2-2L}\right) \qquad (A.50a)$$

$$F_b = \frac{1}{2}\left(\frac{1}{L} + \frac{\cos\theta_R\cos\theta_T}{2-L} + \frac{\sin\theta_R\sin\theta_T}{2L}\right)\ . \qquad (A.50b)$$

As an example, Figure A-4 exhibits F as a function of aspect angle for backscattering by a 10 : 1 prolate spheroid, for both polarizations.

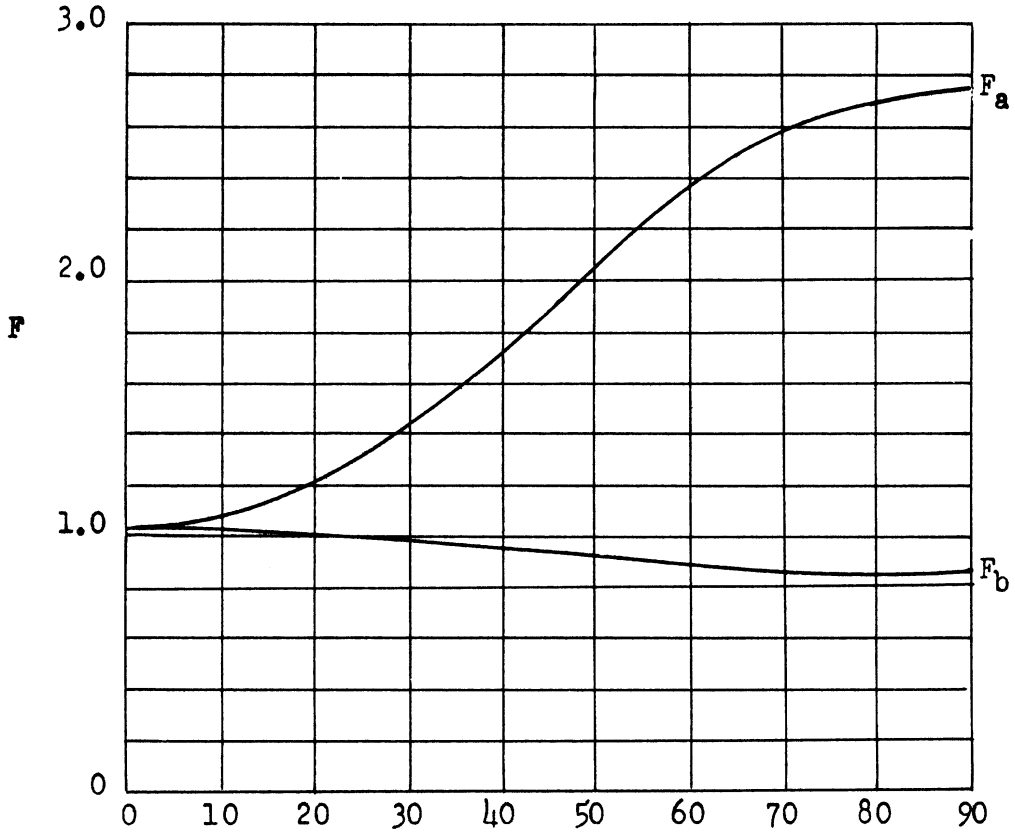

FIG. A-4

Similarly, though more simply, Rayleigh's results for the scattering of a plane scalar wave by a spheroid (Ref. 5) can be generalized to arbitrary incidence. Thus, for a wave of unit amplitude incident along the x - axis, Rayleigh obtains for the Neumann problem (vanishing normal derivative at the body) a scattered wave

$$\psi = -\frac{k^2 V e^{i(kR-\omega t)}}{4\pi R}\left(1+\frac{x}{R}\,\frac{2}{2-L_x}\right) . \qquad (A.51)$$

For a direction of incidence denoted by (θ_T , ϕ_T) and a direction of observation denoted by (θ_R , ϕ_R), this becomes

$$\psi = -\frac{k^2 V e^{i(kR-\omega t)}}{4\pi R}\left(1+\frac{2\sin\theta_R \sin\theta_T \cos\phi_R \cos\phi_T}{2-L_x}\right. \qquad (A.52)$$

$$\left. +\frac{2\sin\theta_R \sin\theta_T \sin\phi_R \sin\phi_T}{2-L_y}+\frac{2\cos\theta_R \cos\phi_T}{2-L_z}\right).$$

Using (A.45) and (A.46), there results a cross-section

$$\sigma' = \frac{4V^2}{4\pi}\left(1+\frac{2\sin\theta_R \sin\theta_T \cos(\phi_R-\phi_T)}{2-L}+\frac{\cos\theta_R \cos\theta_T}{L}\right)^2 \qquad (A.53)$$

APPENDIX B

PHYSICAL OPTICS RADAR CROSS-SECTION OF A FINITE CONE FOR NEAR NOSE-ON ASPECTS

To obtain the monostatic physical optics corss-section of a finite cone for incidence at a small angle, ε, to the axis of symmetry of the cone, we proceed as follows.

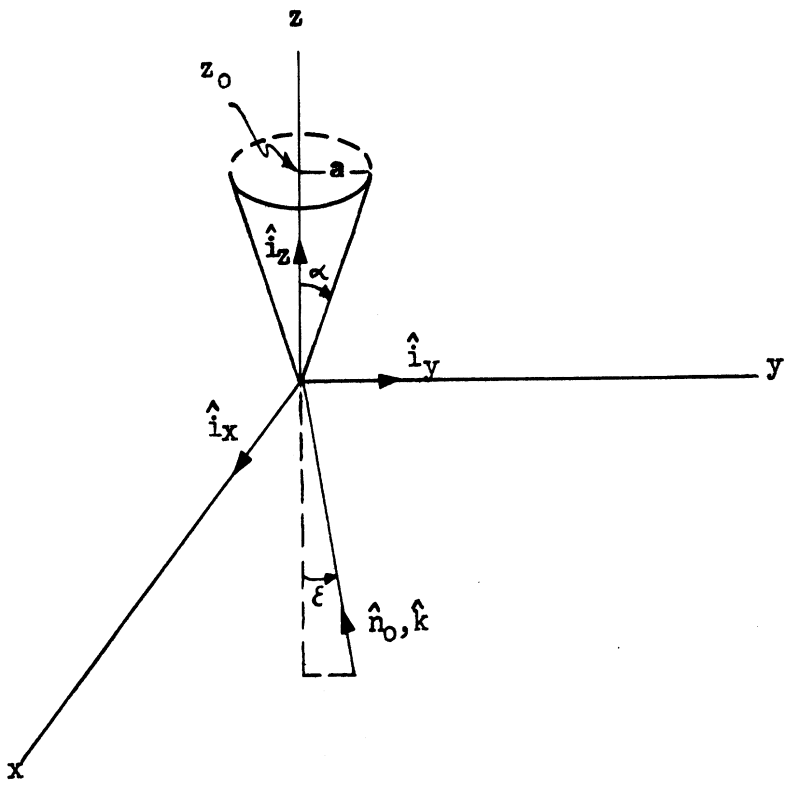

FIG. B-1

Utilizing the physical optics expression for the radar cross-section as given in Reference 1, we obtain

$$\sigma = \frac{4\pi}{\lambda^2} \left| \int_{\substack{\text{illum.} \\ \text{region}}} \hat{n}_o \cdot \hat{n} \; e^{-ik\vec{r}} \cdot (\hat{n}_o + \hat{k}) \; dS \right|^2 \qquad \text{(B.1)}$$

where

$\hat{k} = \hat{n}_o = \cos\varepsilon \, \hat{i}_z + \sin\varepsilon \, \hat{i}_y$ (unit vectors to origin from receiver and transmitter),

a = radius of the base of the cone,

$\hat{n} = -\sin\alpha \, \hat{i}_z + \cos\alpha \cos\phi \, \hat{i}_x + \cos\alpha \sin\phi \, \hat{i}_y$ (normal to cone),

$k = \frac{2\pi}{\lambda}$,

$\vec{r} = z \, \hat{i}_z + z \tan\alpha \cos\phi \, \hat{i}_x + z \tan\alpha \sin\phi \, \hat{i}_y$ (vector from origin to any point on cone),

$\alpha = \frac{1}{2}$ cone angle,

ϕ = angular variable in x-y plane

and

$dS = \frac{z \tan\alpha}{\cos\alpha} \, d\phi dz.$

Because of symmetry, $\hat{n}_o$ and $\hat{k}$ can be chosen in the y-z plane with positive components. From the definitions of $\hat{k}$, $\hat{n}_o$, $\hat{n}$, and $\vec{r}$ we have

$$\hat{n}_o \cdot \hat{n} = -\cos\varepsilon \sin\alpha + \cos\alpha \sin\varepsilon \sin\phi$$

and

$$\vec{r} \cdot (\hat{n}_o + \hat{k}) = 2z(\cos\varepsilon + \tan\alpha \sin\varepsilon \sin\phi).$$

Substituting in Equation B.1 and restricting ε so that $\varepsilon \ll \alpha$, we obtain

$$\sigma = \frac{4\pi}{\lambda^2}\left|\int_0^{2\pi}\int_0^{z_o} \frac{z\tan\alpha}{\cos\alpha}(\cos\alpha\sin\varepsilon\sin\phi - \cos\varepsilon\sin\alpha)e^{-2ikz(\cos\varepsilon+\tan\alpha\sin\varepsilon\sin\phi)}\,dz\,d\phi\right|^2 . \tag{B.2}$$

Setting $b = 2\sin\varepsilon\tan\alpha$ and $c = 2\cos\varepsilon$, we get

$$\sigma = \frac{4\pi}{\lambda^2}\left|\int_0^{2\pi}\tan\alpha(\sin\varepsilon\sin\phi - \tan\alpha\cos\varepsilon)\int_0^{z_o} z\,e^{-ikz(c+b\sin\phi)}\,dz\,d\phi\right|^2 . \tag{B.3}$$

The integration with respect to z can be performed exactly, yielding

$$\sigma = \frac{4\pi}{\lambda^2}\left|\int_0^{2\pi}\tan\alpha(\sin\varepsilon\sin\phi - \tan\alpha\cos\varepsilon)\left(\frac{e^{-ikz_o(b\sin\phi+c)}}{k^2(b\sin\phi+c)^2} + \frac{iz_o e^{-ikz_o(b\sin\phi+c)}}{k(b\sin\phi+c)} - \frac{1}{k^2(b\sin\phi+c)^2}\right)d\phi\right|^2 . \tag{B.4}$$

For $\varepsilon = 0$, (B.4) becomes

$$\sigma = \frac{4\pi}{\lambda^2}\left|\tan^2\alpha\int_0^{2\pi}\left(\frac{e^{-2ikz_o}}{4k^2} + \frac{iz_o e^{-2ikz_o}}{2k} - \frac{1}{4k^2}\right)d\phi\right|^2 \tag{B.5}$$

or upon integrating

$$\sigma = \frac{\pi\tan^4\alpha}{k^2}\left|\frac{1}{2} + ikz_o - \frac{e^{2ikz_o}}{2}\right|^2 \tag{B.6}$$

which is the complete nose-on physical optics cross-section. Neglecting terms of order one in respect to kz_o, Equation B.6 becomes,

$$\sigma = \pi z_o^2 \tan^4 \alpha = \pi a^2 \tan^2 \alpha \qquad (B.7)$$

the well-known nose-on optics approximation.

Returning to the off-nose case, we find that neglecting terms in kb and kc with respect to terms in $(kb)^2$ and $(kc)^2$ and $(kc)^2$ and k^2 bc Equation B.4 becomes

(B.8)

$$\sigma \approx \frac{4\pi}{\lambda^2} \left| \int_0^{2\pi} \frac{z_o \tan\alpha (\sin\varepsilon \sin\phi - \tan\alpha \cos\varepsilon) e^{-ikz_o(b \sin\phi + c)}}{k(b \sin\phi + c)} \, d\phi \right|^2 .$$

Factoring out $\frac{z_o}{k}$ and remembering that

$$b = 2 \sin\varepsilon \tan\alpha, \text{ and}$$

$$c = 2 \cos\varepsilon,$$

we can rewrite Equation B.8 as follows:

$$\sigma \approx \frac{z_o^2}{4\pi} \left| \int_0^{2\pi} \left(1 - \frac{c \sec^2}{b \sin\phi + c}\right) e^{-ikz_o(b \sin\phi + c)} \, d\phi \right|^2 \qquad (B.9)$$

or, since $\left| e^{-ikz_o c} \right| = 1$

$$\sigma \approx \frac{z_o^2}{4\pi} \left| \int_0^{2\pi} \left(1 - \frac{c \sec^2}{b \sin\phi + c}\right) e^{-ikz_o b \sin\phi} \, d\phi \right|^2 . \qquad (B.10)$$

It remains to evaluate the integrals

$$\int_0^{2\pi} e^{-ikz_o\, b \sin\phi}\, d\phi \quad \text{and} \quad \int_0^{2\pi} \frac{e^{-ikz_o b \sin\phi}}{b \sin\phi + c}\, d\phi \ .$$

The first integral is immediately recognizable as a Bessel function.

$$\int_0^{2\pi} e^{-ikz_o\, b \sin\phi}\, d\phi = 2\pi J_o(k\, z_o\, b) \ . \qquad \text{(B.11)}$$

Thus,

$$\sigma = \frac{z_o^2}{4\pi} \left| 2\pi J_o(k\, z_o b) - \int_0^{2\pi} \frac{c \sec^2\alpha\, e^{-ikz_o\, b \sin\phi}}{b \sin\phi + c}\, d\phi \right|^2 \qquad \text{(B.12)}$$

or

$$\frac{\sigma}{\pi a^2} = \frac{1}{\tan^2\alpha} \left| J_o(k\, z_o\, b) - \frac{c \sec^2\alpha}{\pi} \int_0^{\pi} \frac{e^{ikz_o\, b \cos\phi}}{c - b \cos\phi}\, d\phi \right|^2 \qquad \text{(B.13)}$$

which can also be written

$$\frac{\sigma}{\pi a^2} = \frac{1}{\tan^2\alpha} \left| J_o\left(\frac{4\pi z_o \sin\varepsilon \tan\alpha}{\lambda}\right) - \frac{\cos\varepsilon \sec^2\alpha}{\pi} \int_0^{\pi} \frac{e^{i\frac{4\pi z_o \sin\varepsilon \tan\alpha \cos\phi}{\lambda}}}{\cos\varepsilon - \sin\varepsilon \tan\alpha \cos\phi}\, d\phi \right|^2 \qquad \text{(B.14)}$$

For values of $\frac{z_o \sin\varepsilon \tan\alpha}{\lambda} > 1$, the integral in Equation B.8 can be evaluated by the method of stationary phase, yielding

$$\sigma = \frac{\lambda z_o \tan\alpha}{2\pi \sin\varepsilon(\sin^2\varepsilon\tan^2\alpha - \cos^2\varepsilon)^2}\left\{\tan^2\alpha\cos^2\left(\frac{4\pi z_o \sin\varepsilon\tan\alpha}{\lambda} - \frac{\pi}{4}\right)\right. \qquad \text{(B.15)}$$

$$\left. + \frac{\sin^2\varepsilon\cos^2\varepsilon}{\cos^4\alpha}\sin^2\left(\frac{4\pi z_o \sin\varepsilon\tan\alpha}{\lambda} - \frac{\pi}{4}\right)\right\}$$

which we observe is the asymptotic form of

$$\frac{\sigma}{\pi a^2} = \frac{\tan^2\alpha\left[J_o\left(\frac{4\pi z_o \sin\varepsilon\tan\alpha}{\lambda}\right)\right]^2 + \frac{\sin^2\varepsilon\cos^2\varepsilon}{\cos^4\alpha}\left[J_1\left[\frac{4\pi z_o \sin\varepsilon\tan\alpha}{\lambda}\right)\right]^2}{(\sin^2\varepsilon\tan^2\alpha - \cos^2\varepsilon)^2} . \qquad \text{(B.16)}$$

It is noted that while the nose-on physical optics cross-section is independent of wavelength, the stationary phase result indicates that the near nose-on cross-section varies linearly with wavelength. However, it must be remembered that for small values of ε, α and $\frac{z_o}{\lambda}$ ($\varepsilon < \alpha$, $\alpha < 10^o$, $\frac{z_o}{\lambda} < 10$) the integrand in Equation B.8 or B.14 does not oscillate rapidly enough for valid application of stationary phase. The integral in Equation B.14 was therefore evaluated on an analog computer for various values of α, ε, and z_o/λ. The results are compared with the results computed from Equations B.15 and B.16 in the Figures B-2 through B-7.

The figures indicate that the modified form of the stationary phase result, Equation B.16, is a better approximation than the stationary phase result itself, Equation B.15. The figures also indicate that the requirement

$$\frac{4\pi\, z_o \sin\varepsilon\tan\alpha}{\lambda} \gg 1$$

can be relaxed considerably.

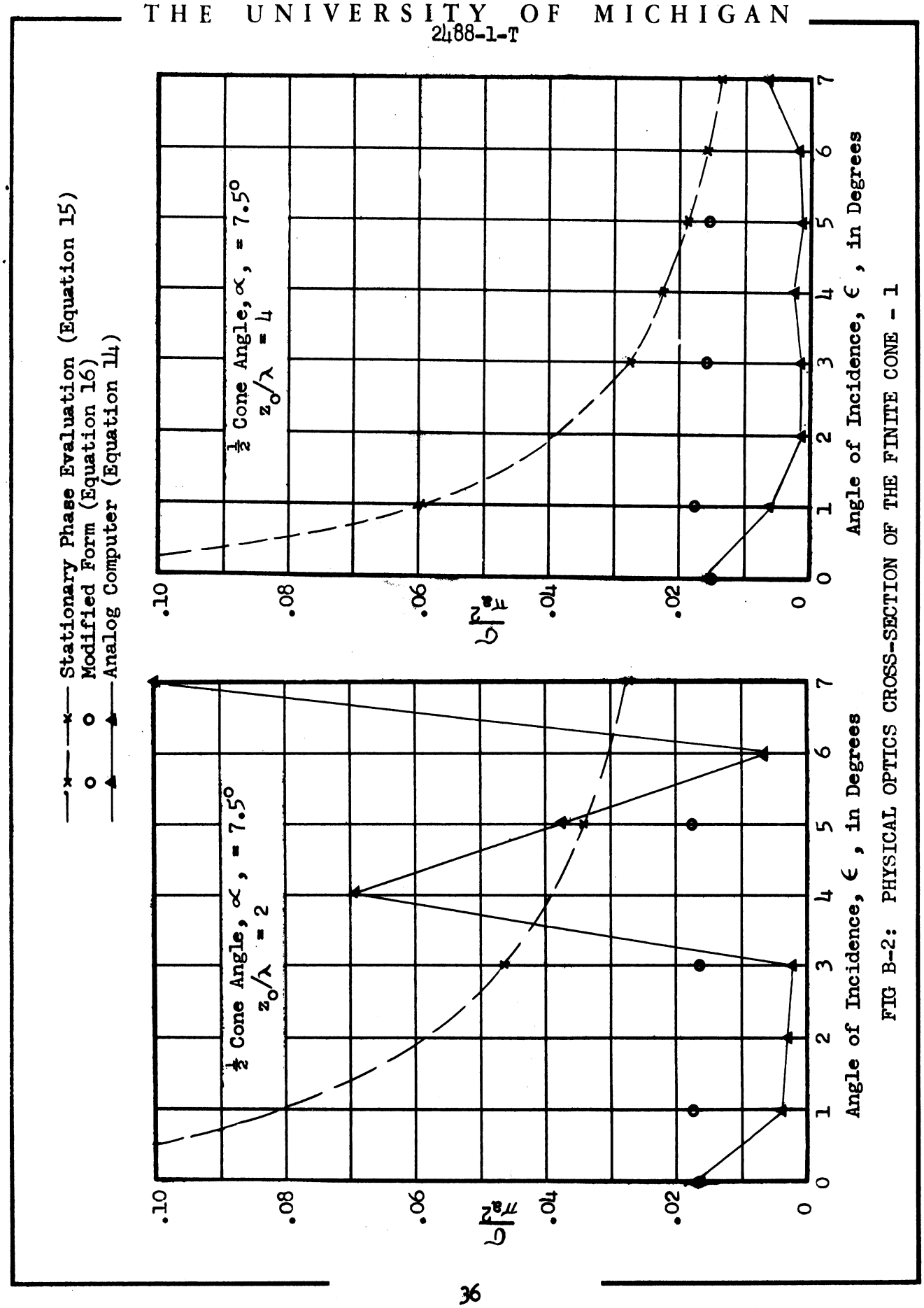

FIG B-2: PHYSICAL OPTICS CROSS-SECTION OF THE FINITE CONE - 1

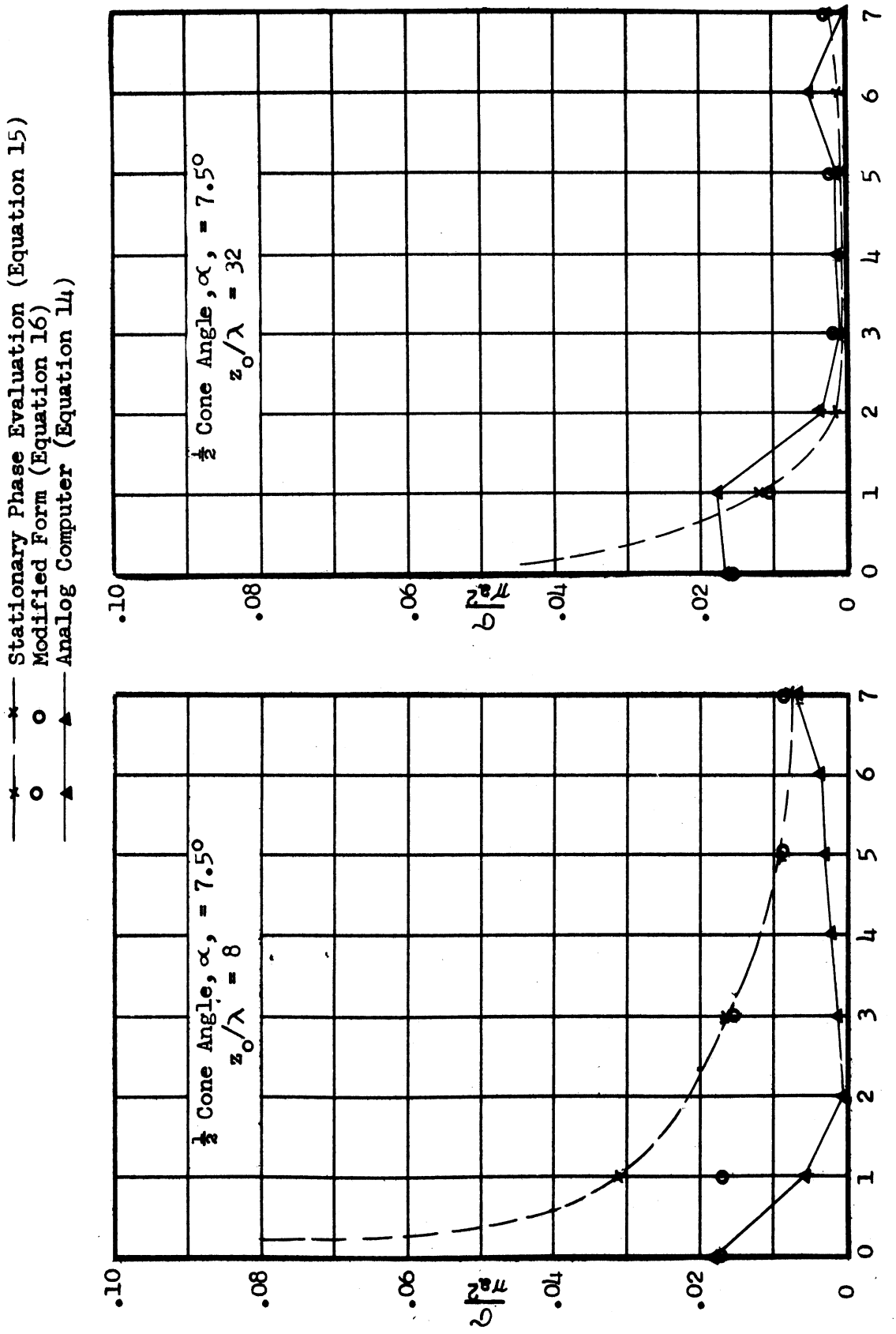

FIG B-3: PHYSICAL OPTICS CROSS-SECTION OF THE FINITE CONE - 2

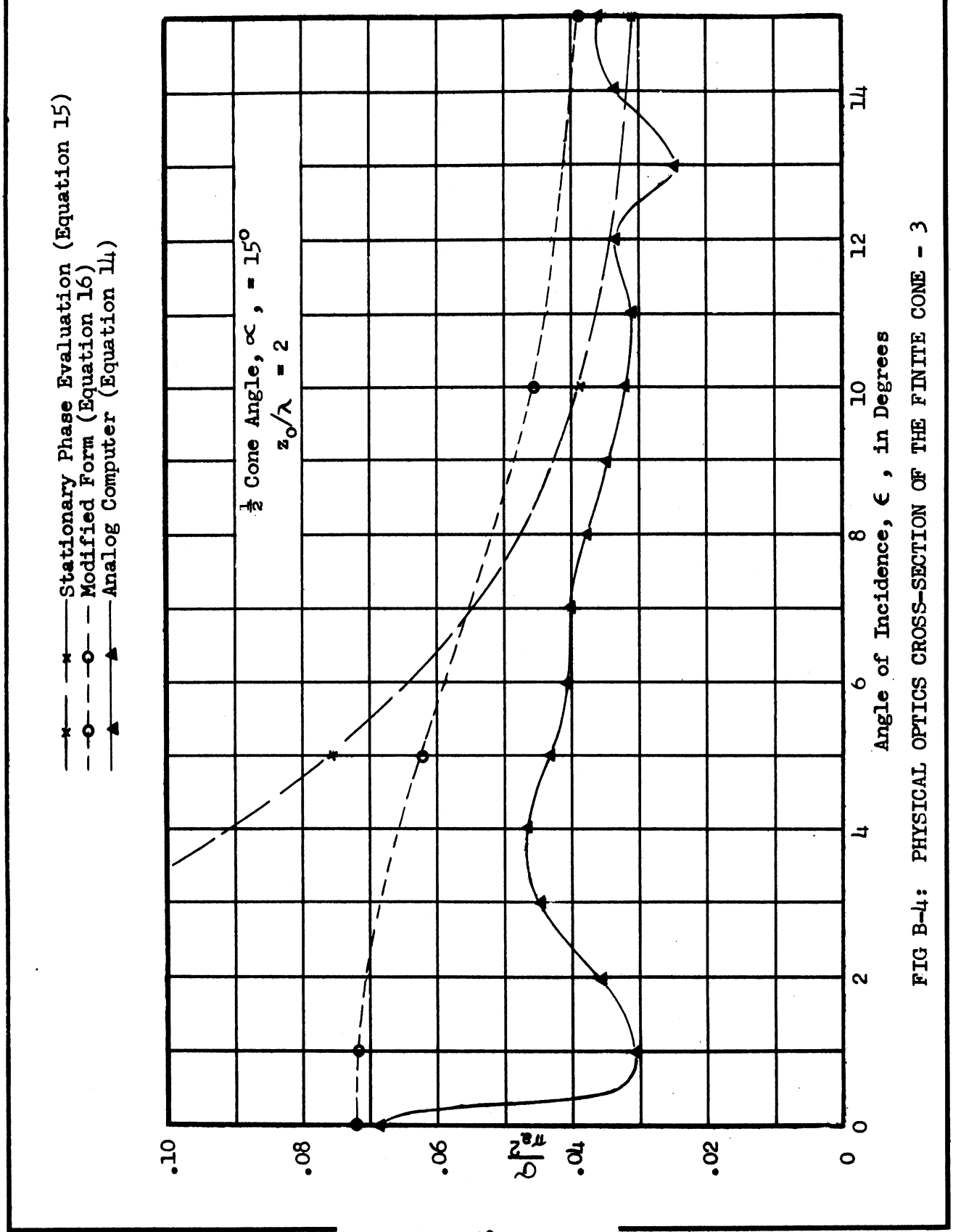

FIG B-4: PHYSICAL OPTICS CROSS-SECTION OF THE FINITE CONE - 3

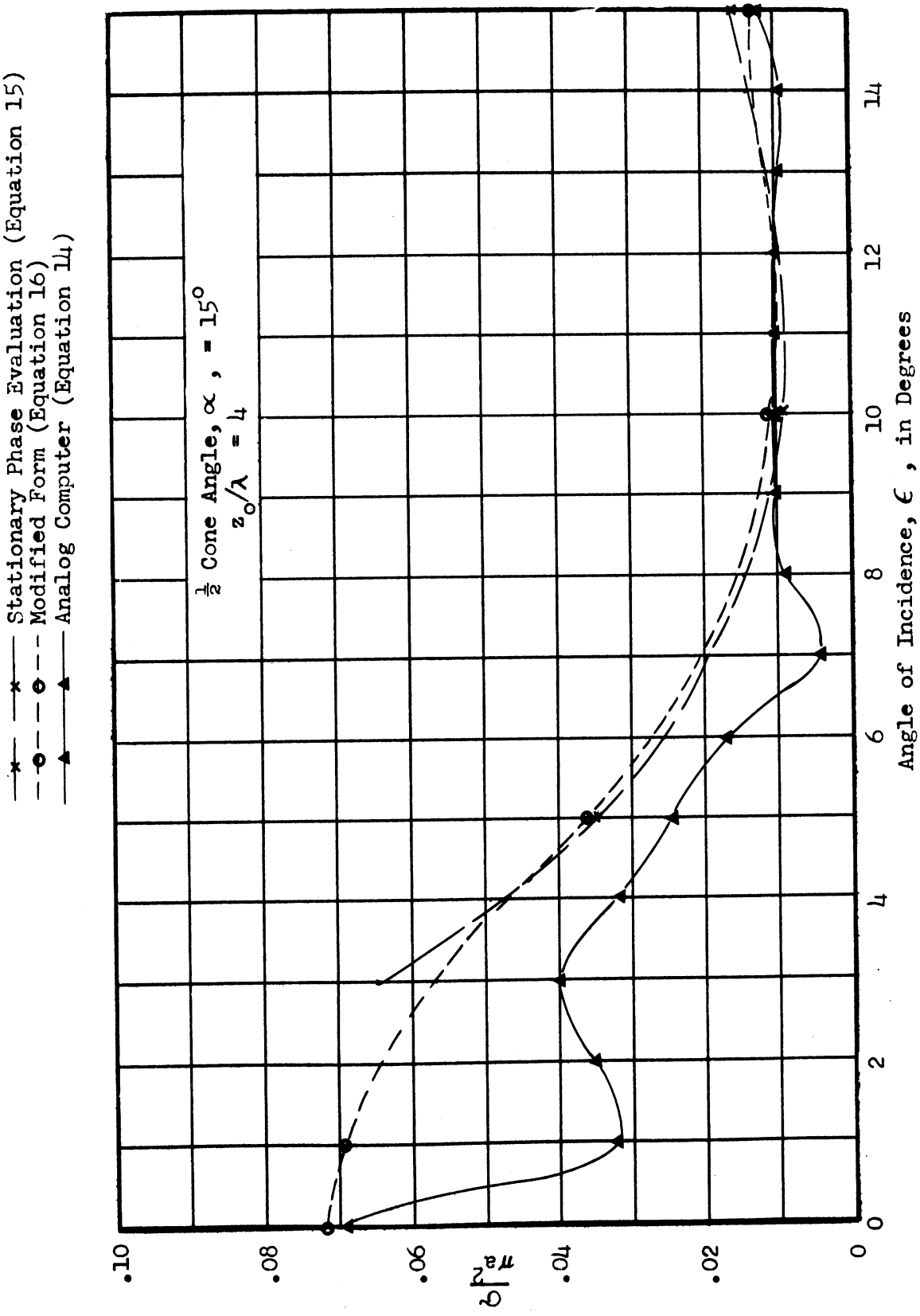

FIG B-5: PHYSICAL OPTICS CROSS-SECTION OF THE FINITE CONE - 4

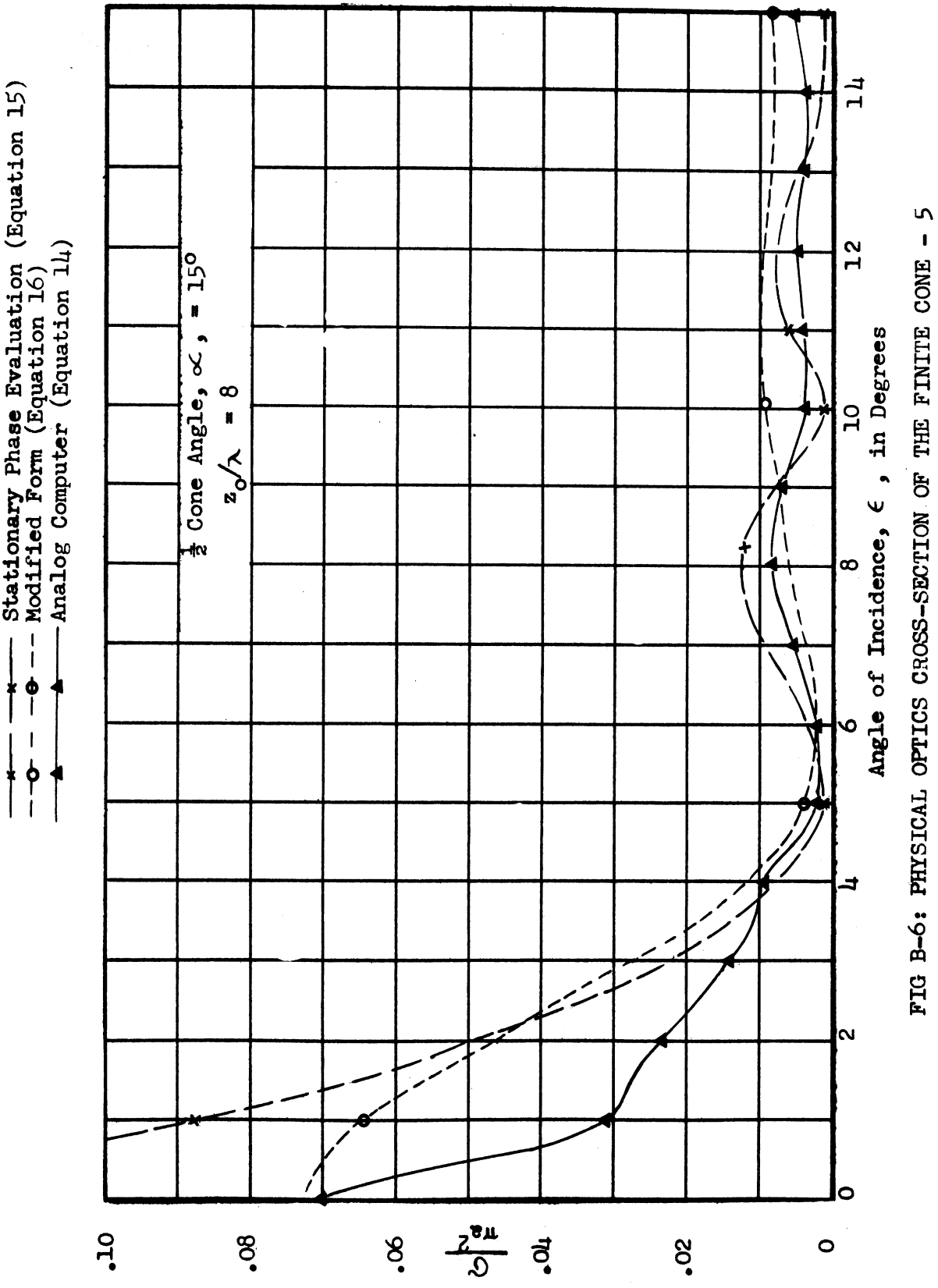

FIG B-6: PHYSICAL OPTICS CROSS-SECTION OF THE FINITE CONE - 5

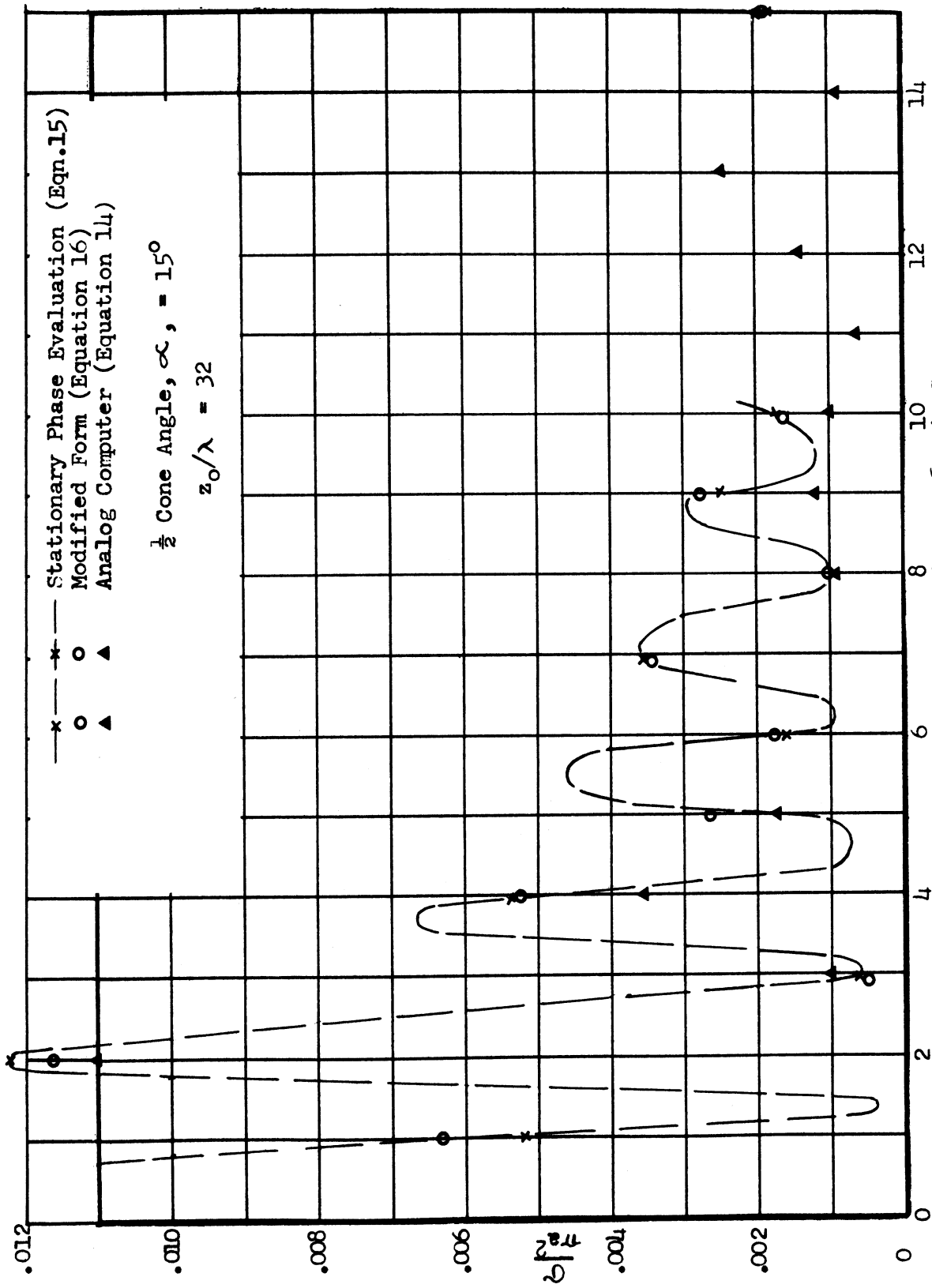

FIG B-7: PHYSICAL OPTICS CROSS-SECTION OF THE FINITE CONE - 6

APPENDIX C

THE RADAR CROSS-SECTION OF A THIN WIRE LOOP FOR SMALL WAVELENGTHS

The radar cross-section of a thin wire loop is derived, for wavelengths which are small compared with the radius of the loop and large compared with the radius of the wire, using an expression due to Chu (Ref. 3) for straight wires.

Chu's expression, for incidence normal to the wire becomes

$$\sigma = \frac{\pi L^2 \cos^4 \phi}{\left(\frac{\pi}{2}\right)^2 + \left(\log \frac{\lambda}{\gamma \pi b}\right)^2} \qquad (C.1)$$

where

L = length of wire,

ϕ = angle between electric vector and the plane of the wire and the incident direction,

γ = Euler's constant ≈ 1.78 and

b = radius of wire.

Since $\sigma = 4\pi r^2 \left| \frac{\vec{E}_s}{\vec{E}_i} \right|^2$, we can obtain an expression for $\vec{E}_s$ except for phase from (C.1) assuming $|\vec{E}_i| = 1$ and Huygen's principle holds.

$\vec{E}_s$ then has the form

$$\vec{E}_s = \frac{\vec{s}\, L \cos^2 \phi}{2\left\{\left(\frac{\pi}{2}\right)^2 + \left(\log \frac{\lambda}{\gamma \pi b}\right)^2\right\}^{\frac{1}{2}}} \frac{e^{ikr}}{r}$$

where $\vec{s}$ is a unit vector in an arbitrary direction.

Setting $L = ad\phi$ (where a is the radius of the loop) and integrating around the loop we obtain

$$\vec{E}_s = \frac{\vec{s}\ e^{ikr}\ a}{2r\left\{\left(\frac{\pi}{2}\right)^2 + \left(\log\frac{\lambda}{\gamma\pi b}\right)^2\right\}^{1/2}} \int_0^{2\pi} \cos^2\phi\, d\phi$$

$$= \frac{\vec{s}\ \pi\ a\ e^{ikr}}{2r\left\{\left(\frac{\pi}{2}\right)^2 + \left(\log\frac{\lambda}{\gamma\pi b}\right)^2\right\}^{1/2}} .$$

The cross-section of the loop can then be written

$$\sigma = 4\pi r^2 \left|\frac{\vec{E}_s}{\vec{E}_i}\right|^2$$

$$= \frac{\pi^3\ a^2}{\left(\frac{\pi}{2}\right)^2 + \left(\log\frac{\lambda}{\gamma\pi b}\right)^2} .$$

APPENDIX D

CIRCULAR WEDGE APPROXIMATION TO RADAR CROSS-SECTION OF THIN FINITE CONES

The radar cross-section of a thin finite cone is determined by considering only the contribution from the base which is approximated by a circular wedge shape. That this approximation retains the essential scattering characteristics of the cone is indicated by first computing the cross-section of the approximating wedge shape using physical optics. It is seen that the result thus obtained and the physical optics thin cone result (Equation B.7) agree exactly.

The circular wedge cross-section is then computed using a method suggested by C. E. Schensted (Ref. 7). Expressions for the field due to a straight wedge, which are in general more exact than physical optics, are employed.

Proceeding as outlined, using the physical optics expressions in Reference 1, we obtain the following expressions for the scattered magnetic field from a semi-infinite wedge of length L with incidence perpendicular to the back face as shown in Figure D-1:

$$\vec{H}_s = \frac{e^{-ikR'}}{R'} \left[-\frac{ik}{2\pi} \left(\hat{n}_o \cdot \vec{f} \right) \hat{a} \right]$$

where

$$\vec{f} = \int_{\text{illuminated area}} \hat{n}\, e^{-ik\vec{r}\left(\hat{n}_o + \hat{k}\right)} dS ,$$

$\vec{H}_i$ = unit incident field = $\hat{a}$,

$\hat{n}_o = \hat{k} = \hat{i}_z$,

$\hat{n}$ = normal to wedge = $\hat{i}_x \sin\gamma - \hat{i}_z \cos\gamma$,

γ = included wedge angle,

and $dS = \frac{dydx}{\cos\gamma}$

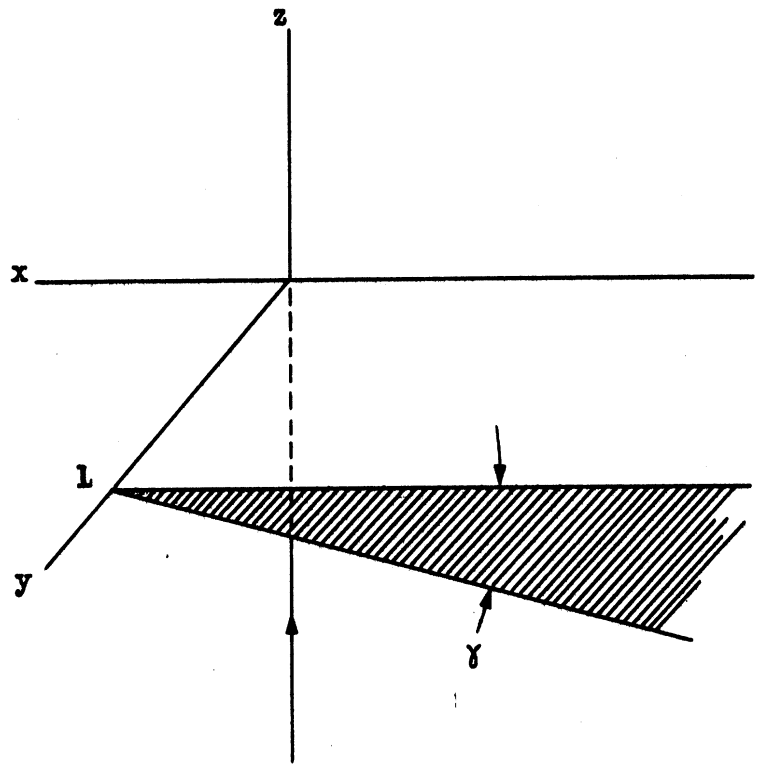

FIG D-1

Hence $\vec{r} = \hat{i}_x x + \hat{i}_y y + \hat{i}_z (x \tan\gamma)$,

$\hat{n} \cdot \vec{n}_o = - \cos\gamma$,

and $\vec{r} \cdot (\vec{n}_o + \vec{k}) = 2x \tan\gamma$.

Thus,

$$\vec{n}_o \cdot \vec{f} = - \int_0^{-\infty} \int_0^{L} e^{-i2kx\tan} \, dy dx$$

$$= L \int_0^{\infty} e^{+i2kx\tan} \, dx$$

$$= + L \left[\frac{e^{+i2kx\tan\gamma}}{i2k\tan\gamma} \right]_0^{\infty} .$$

Associating the edge contribution with the value at the lower limit (just as in the infinite cone case we obtain the "tip" contribution) we have finally

$$\vec{n}_o \cdot \vec{f} = \frac{- L}{i2k\tan\gamma}$$

and

$$\vec{H}_s = + \frac{L \hat{\phi}}{4\pi\tan\gamma} \frac{e^{-ikR'}}{R'} .$$

Now letting $L = a d\beta$,where a = radius of base,and integrating around the base (a = constant vector),we obtain

$$\vec{H}_s = \int_0^{2\pi} \frac{\hat{a}\, e^{-ikR'}}{4\pi R \tan\gamma}\, a\,d\beta = \frac{a\,\hat{a}\, e^{-ikR'}}{2R' \tan\gamma}$$

$$\sigma = 4\pi R'^2 \left| \frac{\vec{H}_s}{\vec{H}_i} \right|^2$$

$$= 4\pi R'^2 \left| \frac{a\ e^{-ikR'}}{2R' \tan\gamma}\ \hat{a} \right|^2$$

$$= \frac{\pi a^2}{\tan^2\gamma} \quad .$$

But $\gamma = \frac{\pi}{2} - \alpha$ (see Fig. D-2) where α is half the cone angle; thus,

$$\tan\alpha = \tan\left(\frac{\pi}{2} - \gamma\right)$$

$$= \cot\gamma$$

and finally

$$\sigma = \pi a^2 \tan^2\alpha \quad ,$$

which is precisely the nose-on result obtained for the cone directly with physical optics.

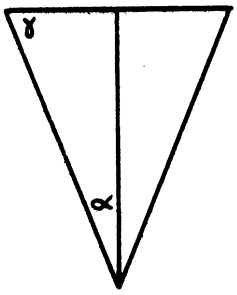

FIG D-2

Now instead of using the physical optics field for a wedge, we use the generally more exact expression as presented in Reference 7, and proceed exactly as before. For linear polarization the scattered field for a wedge of length L is

$$\vec{E}_s = \frac{L\, e^{ikr}}{4r\phi_o} \sin\frac{\pi^2}{2\phi_o} \left[\frac{E(a)\hat{\phi} - E(b)\hat{k}}{A} - \frac{E(a)\hat{\phi} + E(b)\hat{k}}{B} \right], \qquad (D.1)$$

where

E(a) = component of the incident field perpendicular to the edge of the wedge,

E(b) = component of the incident field parallel to the edge of the wedge,

$A = \cos\frac{\pi\theta}{\phi_o} + \cos\frac{\pi^2}{2\phi_o}$

$B = 1 - \cos\frac{\pi^2}{2\phi_o}$

ϕ_o = wedge angle (see Fig. D-3) where in terms of the half cone angle

$$\phi_o = \frac{3\pi}{4} + \frac{\alpha}{2}$$

θ = angle of incidence, and

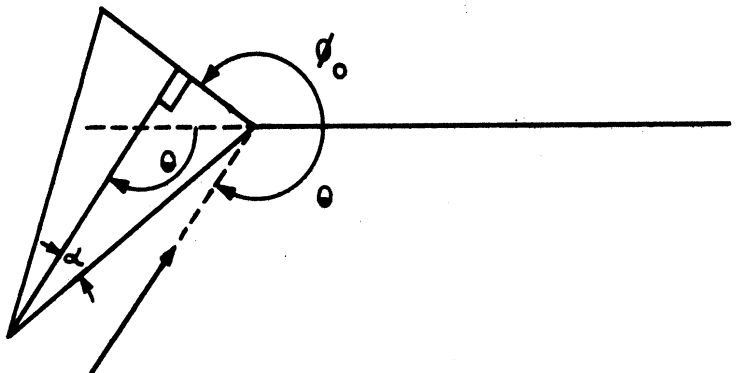

FIG D-3

$\hat{\phi}$ and $\hat{k}$ are unit vectors perpendicular and parallel, respectively, to the edge of wedge (or circumference of the cone base) (see Fig. D-4)

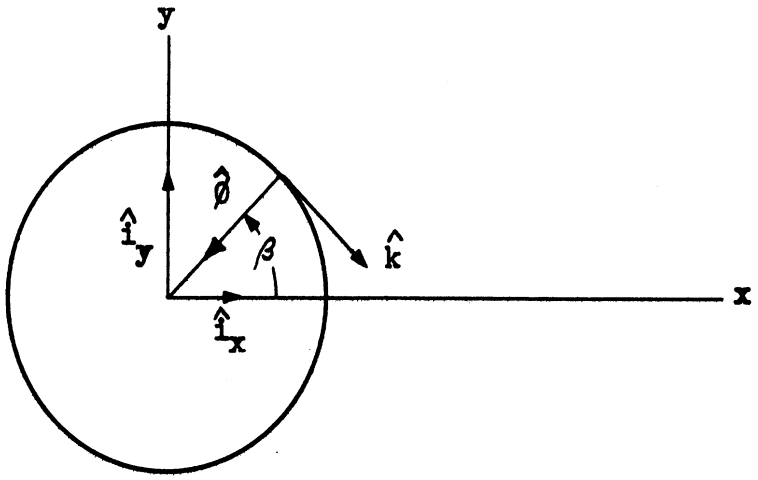

Figure D-4

The quantities $\hat{\phi}$ and $\hat{k}$ are related to $\hat{i}_x$ and $\hat{i}_y$ as follows:

$$\hat{\phi} = -\hat{i}_x \cos\beta - \hat{i}_y \sin\beta \qquad \hat{i}_x = -\hat{\phi}\cos\beta + \hat{k}\sin\beta \qquad \text{(D.2)}$$

$$\hat{k} = \hat{i}_x \sin\beta - \hat{i}_y \cos\beta \qquad \hat{i}_y = -\hat{\phi}\sin\beta - \hat{k}\cos\beta$$

Since the incident electric vector lies in the x-y plane and since the base of the cone is symmetric about the origin in the x-y plane, we may choose $\vec{E}_{incident}$ to lie along $\hat{i}_x$.

Thus,

$$\hat{E}_i = \hat{i}_x = -\hat{\phi}\cos\beta + \hat{k}\sin\beta = E(a)\hat{\phi} + E(b)\hat{k} \quad . \qquad \text{(D.3)}$$

To obtain the total scattered field we compute the field for a wedge of length $L = ad\beta$ where a is the radius of the base of the cone, and integrate around the base.

Thus, we have from (D.1) and (D.3)

$$\vec{E}_s = \int_0^{2\pi} \frac{a\, e^{ikr}}{4r\phi_o} \sin\frac{\pi^2}{2\phi_o} \left[\frac{-\cos\beta\,\hat{\phi} - \sin\beta\,\hat{k}}{\cos\frac{n\theta}{\phi_o} + \cos\frac{\pi^2}{2\phi_o}} - \frac{-\cos\beta\,\hat{\phi} + \sin\beta\,\hat{k}}{1 - \cos\frac{\pi^2}{2\phi_o}} \right] d\beta$$

Using Equations (D.2) we get

$$\vec{E}_s = \frac{a\, e^{ikr}}{4\, r\, \phi_o} \sin\frac{\pi^2}{2\phi_o} \int_0^{2\pi} \left[\frac{\hat{i}_x \cos 2\beta + \hat{i}_y \sin 2\beta}{\cos\frac{n\theta}{\phi_o} + \cos\frac{\pi^2}{2\phi_o}} - \frac{\hat{i}_x}{1 - \cos\frac{\pi^2}{2\phi_o}} \right] d\beta$$

$$= -\frac{a\pi e^{ikr}}{2\, r\, \phi_o} \sin\frac{\pi^2}{2\phi_o} \frac{\hat{i}_x}{1 - \cos\frac{\pi^2}{2\phi_o}} \quad .$$

The effective radar cross-section is defined by

$$\sigma = \lim_{r \to \infty} 4\pi r^2 \left| \frac{\vec{E}_s \cdot \hat{p}}{\vec{E}_i} \right|^2$$ where $\hat{p}$ = receiver polarization vector

In the case being considered, $\hat{p} = \hat{i}$ and $|\vec{E}_i| = 1$. Thus,

$$\sigma = \lim_{r \to \infty} 4\pi r^2 \left| \vec{E}_s \right|^2 \quad .$$

Substituting for $\vec{E}_s$, we get

$$\sigma = \frac{a^2 \pi^3}{\phi_o^2} \frac{\sin^2 \frac{\pi^2}{2\phi_o}}{\left(1 - \cos \frac{\pi^2}{2\phi_o}\right)^2}$$

$$= \frac{a^2 \pi^3}{\phi_o^2} \cot^2 \frac{\pi^2}{4\phi_o}$$

or, in terms of the half cone angle, α,

$$\frac{\sigma}{\pi a^2} = \frac{\pi^2}{\left(\frac{3\pi}{4} + \frac{\alpha}{2}\right)^2} \cot^2 \left(\frac{\pi^2}{3\pi + 2\alpha}\right) . \qquad (D.4)$$

This result is compared with the physical optics result in Figure D-7. This method can be applied to any body with a ring singularity. Consider, for example, a cone-cylinder combination (Fig. D-5) viewed nose-on.

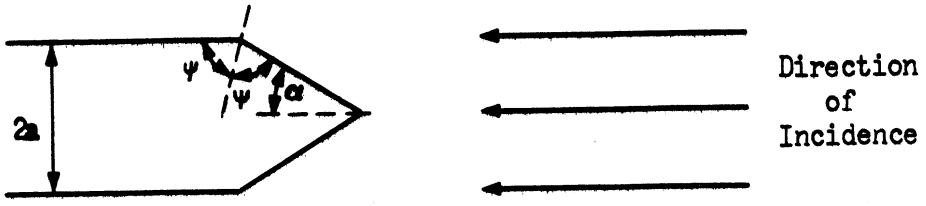

$\psi = \pi - \phi_o$ Figure D-5

The expression derived for the cross-section

$$\frac{\sigma}{\pi a^2} = \frac{\pi^2}{\phi_o^2} \cot^2 \frac{\pi^2}{4\phi_o} \qquad (D.5)$$

still applies. In terms of the half cone angle, α, we have

$$\frac{\sigma}{\pi a^2} = \frac{\pi^2}{\left(\frac{\pi}{2} + \frac{\alpha}{2}\right)^2} \cot^2\left(\frac{\pi^2}{2(\pi + \alpha)}\right) \qquad (D.6)$$

Similarly, for the contribution from any ring singularity, Equation D.5 holds where ϕ_0 is the supplement of half of the included wedge angle (Fig. D-6)

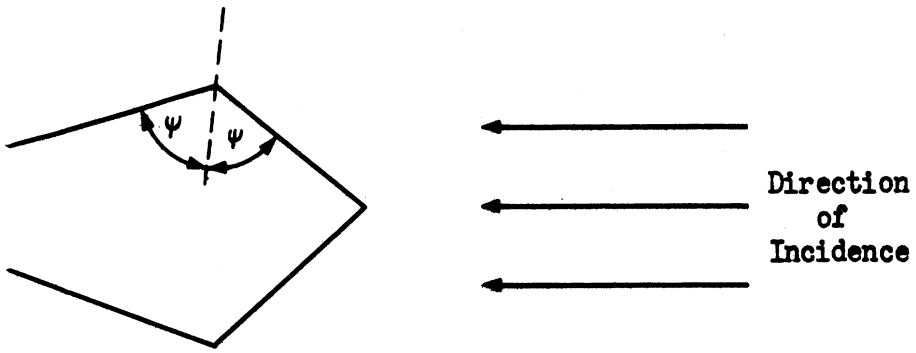

$\psi = \pi - \phi_0$

Figure D-6

Equations D.4, D.5, and D.6 are plotted in Figure D-8.

SECRET

$$Y_1 = \frac{\pi}{\left(\frac{3\pi}{4} + \frac{\alpha}{2}\right) \tan\left(\frac{\pi^2}{3\pi + 2\alpha}\right)} = \sqrt{\frac{\sigma_{wedge}}{\pi a^2}}$$

$$Y_2 = \tan \alpha = \sqrt{\frac{\sigma_{phys.\ op.}}{\pi a^2}}$$

$\alpha = \frac{1}{2}$ cone angle

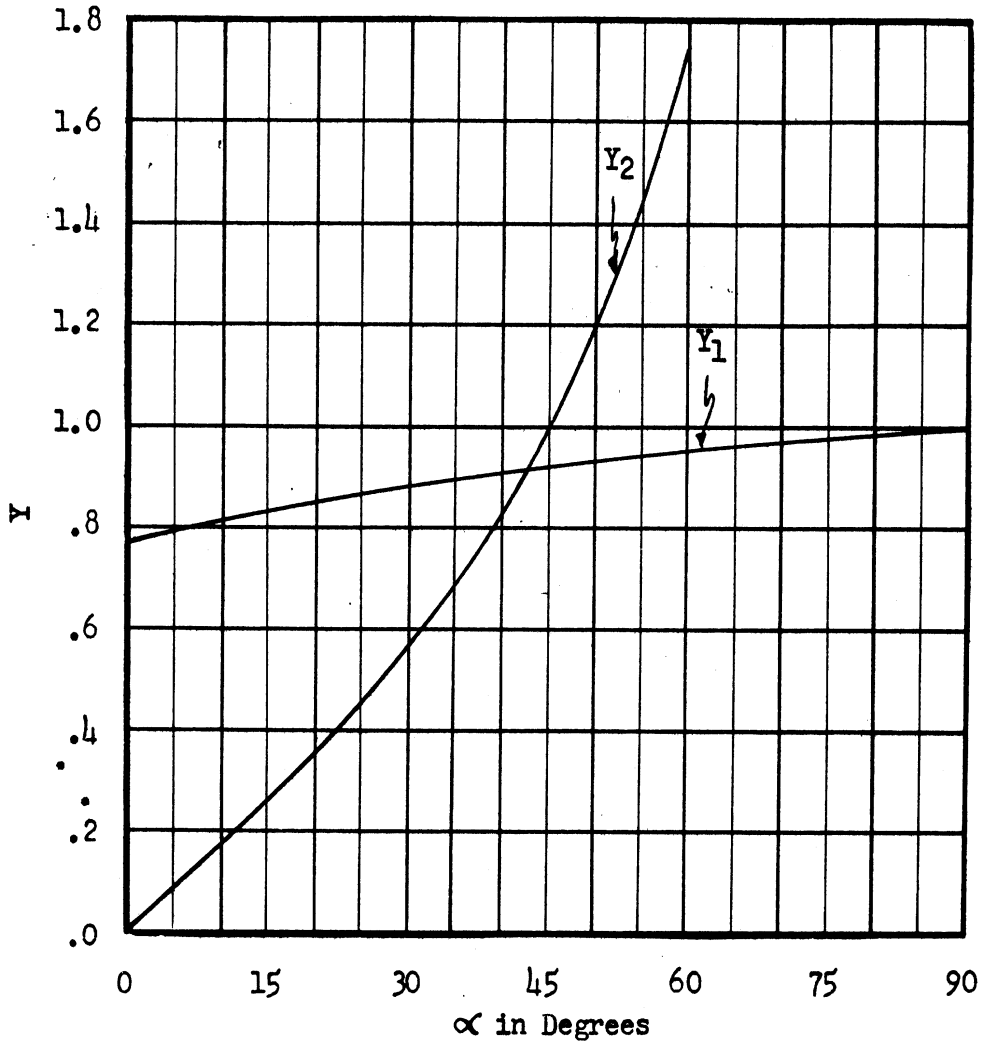

FIG. D-8 NOSE-ON FINITE CONE CROSS-SECTIONS AS COMPUTED BY PHYSICAL OPTICS AND CIRCULAR WEDGE APPROXIMATIONS.

SECRET

UNCLASSIFIED when
Appendices E and F
are removed.

SECRET

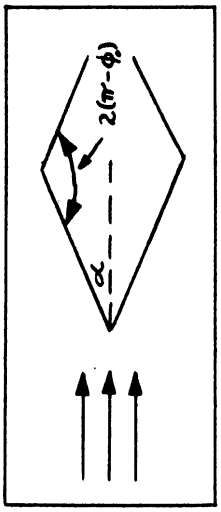

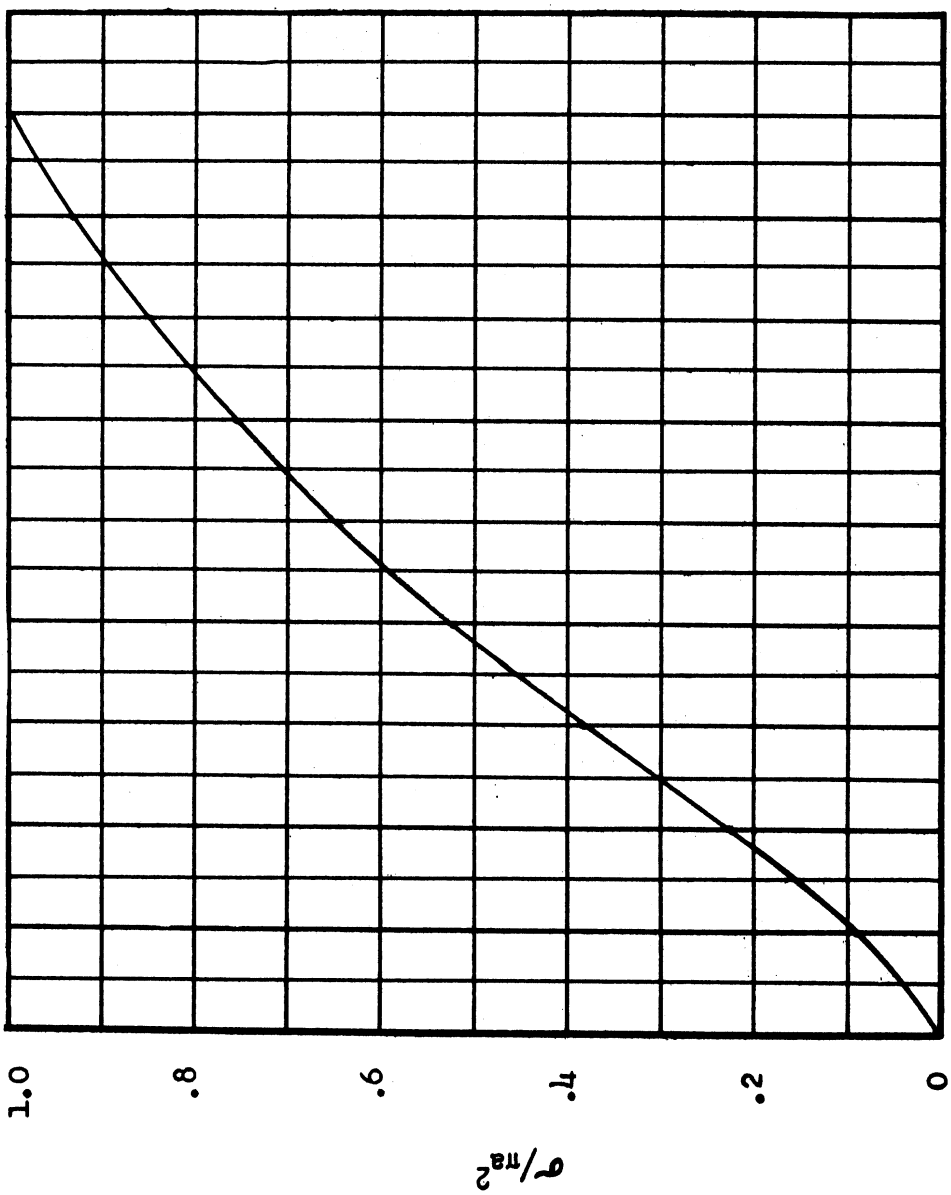

FIG. D-8 NOSE-ON CROSS-SECTION OF CIRCULAR WEDGE

SECRET

REFERENCES TO UNCLASSIFIED PART OF THE REPORT (THROUGH APPENDIX D)

1. K. M. Siegel, H. A. Alperin, R. R. Bonkowski, J. W. Crispin, Jr., A. L. Maffett, C. E. Schensted and I. V. Schensted, "Studies in Radar Cross-Sections VIII - Theoretical Cross-Section as a Function of Separation Angle Between Transmitter and Receiver at Small Wavelengths", The University of Michigan, Engineering Research Institute, (UMM-115, October 1953), UNCLASSIFIED.

2. A. F. Stevenson, "Solution of Electromagnetic Scattering Problems as Power Series in the Ratio (Dimension of Scatterer)/Wavelength", Journal of Applied Physics, 24, 1134 (1953).

3. J. H. Van Vleck, F. Bloch, and M. Hamermesh, "Theory of Radar Reflection from Wires or Thin Metallic Strips", Journal of Applied Physics, 18, 274, (1947).

4. R. G. Kouyoumjian, "The Backscattering from a Circular Loop", The Ohio University State Research Foundation Report No. 662-5 (1956). UNCLASSIFIED.

5. Strutt, J. W., Baron Rayleigh, "On the Incidence of Aerial and Electric Waves Upon Small Obstacles in the Form of Ellipsoids or Elliptic Cylinders, and on the Passage of Electric Waves Through a Circular Aperture in a Conducting Screen", Phil. Mag., 44, (1897).

6. Stratton, J. A., Electromagnetic Theory, McGraw-Hill, New York, pp. 432-435 (1941).

7. A. L. Maffett, M. L. Barasch, W. E. Burdick, R. F. Goodrich, W. C. Orthwein, C. E. Schensted, and K. M. Siegel, "Studies in Radar Cross-Sections XVII - Complete Scattering Matrices and Circular Polarization Cross-Sections for the B-47 Aircraft at S-Band,", The University of Michigan, Engineering Research Institute, (2260-6-T, June 1955). CONFIDENTIAL.

APPENDIX E

MINIMAL CROSS-SECTION SHAPES

For many years the author has advocated that missile design should be conducted from a radar cross-section point of view. The objective would be to design an offensive missile whose cross-section is minimal for any set of Coefficients of Drag and Lift vs. Mach Number and Reynolds Number given as restrictions which the geometry must obey. It was pointed out that the minimum cross-section one could expect a missile made of a conducting material to equal or approach was (for small wavelengths) the radar cross-section of an infinite cone. It was believed that infinite cones would give the same results as smoothly terminated bodies for which the cone was the tangent surface.

This belief was verified theoretically for small wavelengths by Schiff (Ref. E1) for the ogive, and experimentally for thick ogives by Sletten (Ref. E2). The question remained as to how sharp one could terminate the conical body and still obtain a nose-on answer which was of the same order of magnitude as the cross-section of an infinite cone,

$$\sigma \doteq \frac{\lambda^2 \tan^4 \alpha}{16\pi} \quad .$$

For thick bodies is was found that the termination could involve much smaller radii of curvature than for thin bodies. In fact for thin ogives the Fock reasoning (discussed below) is only valid for very small λ/R ratios, where R is the radius of curvature in the plane of Poynting's vector at the shadow boundary (the curve on the body which separates the

lit region of the body from the shadow region). This has been indicated by recent experiments conducted at The Ohio State University (Ref. E3), which give nose-on cross-sections for thin ogives much different from the infinite cone answer, and by recent Air Force Cambridge Research Center experiments. Thus, the cross-sections of thin bodies for which $\lambda/R \approx 0.1$ are not predictable by physical optics. The cross-sections of such bodies are expected to be larger on the average than those predicted by optics formulas. Nevertheless such smooth terminations tend to reduce the cross-section.

Here we shall consider the back-scattering cross-section of a finite cone with various base terminations for illumination along the cone axis. This cross-section will depend critically on the method of termination at the base of the cone. Hence, we attempt to isolate the contribution of the cap of the cone from that of the tip. Quite generally we find that the contribution of the base depends upon the rapidity of the transition from light to shadow measured in terms of the wavelength.

The finite cone itself has been discussed in the preceding appendices; here we will examine a finite cone smoothly fitted with a spherical cap. For a wavelength of the same order as the length of the cone we cannot treat the contributions of the tip and the base as uncoupled. However, if the wavelength is decreased so that the distance between the tip and the shadow boundary is several wavelengths, we expect to be able to treat the contributions as virtually uncoupled.

If the radius of curvature at the shadow boundary is large with respect to the wavelength, the base contribution to the cross-section is found

by Schiff (Ref. E1) to be of higher order in λ than that from the tip. As the radius of curvature of the shadow boundary decreases in terms of wavelength, the base contribution becomes increasingly important until in the limit of vanishing radius of curvature (i.e., an ordinary finite cone) the dominant contribution to the cross-section comes from the base.

In applying the physical optics approximation to the finite cone, it is found that there is one term that can be identified as the tip contribution. There is also a term arising from the assumption that the current on the body is discontinuous at the shadow boundary. This latter term, the base contribution, is present even when the body is smoothly terminated and the discontinuity in current is known to be nonexistent. However, the tip contribution is still valid. Thus the cross-section of smoothly terminated cones will consist of the physical optics tip contribution plus a contribution arising from an adequate treatment of the base. This base contribution, it will be recalled, increases in relation to the complete cross-section as the radius of curvature of the shadow boundary decreases.

One method of determining the base contribution, in the special case when the cone has a spherical cap (see Fig. E-1) is obtained from a consideration of the exact sphere solution.

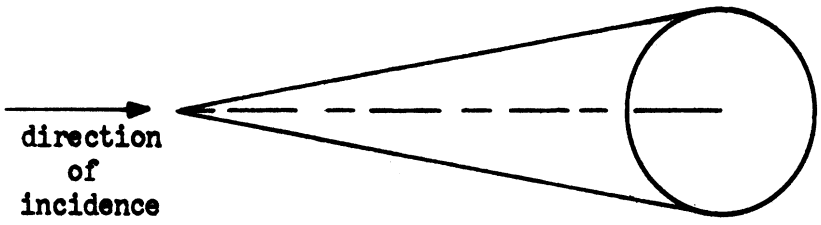

FIG E-1: A CONE CAPPED BY A SPHERE

The sphere cross-section can be decomposed into a geometrical optics term plus a diffraction term. This has been done by Franz, Deppermann, and Imai (Refs. E4 and E5). The optics term comes from the region of specular reflection and the diffraction term from the effects of the currents induced in the shadow and near the shadow boundary. This considration leads us to attempt to approximate the base contribution of the spherically capped cone by determining the differences between the total field due to the sphere and its geometric optics field. This approach was carried out by Pound recently at the Cornell Aeronautical Laboratory, Inc. (Ref. E6) and here at The University of Michigan in 1954 (Ref. E7). These two estimates are shown graphically in Figure E-2.

No such ready solutions to the problems posed by a smoothly fitted convex cap which is otherwise arbitrary are available. However, Fock (Ref. E8) has developed a modification of geometric optics which arises from a local analysis of the field in the shadow region and leads to a smooth transition from light to shadow for the field induced on the surface. From the work of both Franz and Fock we see that the important parameter in determining the contribution of the diffraction term is the radius of curvature at the shadow boundary as compared with the wavelength.

An equivalent spherical cap is thus determined and its contribution to the cross-section can be found using the technique as outlined previously. If the radius of curvature at the shadow boundary does not change rapidly as the shadow region is entered, this approximation will yield good results.

Using the "average" expression for the contribution from the base as

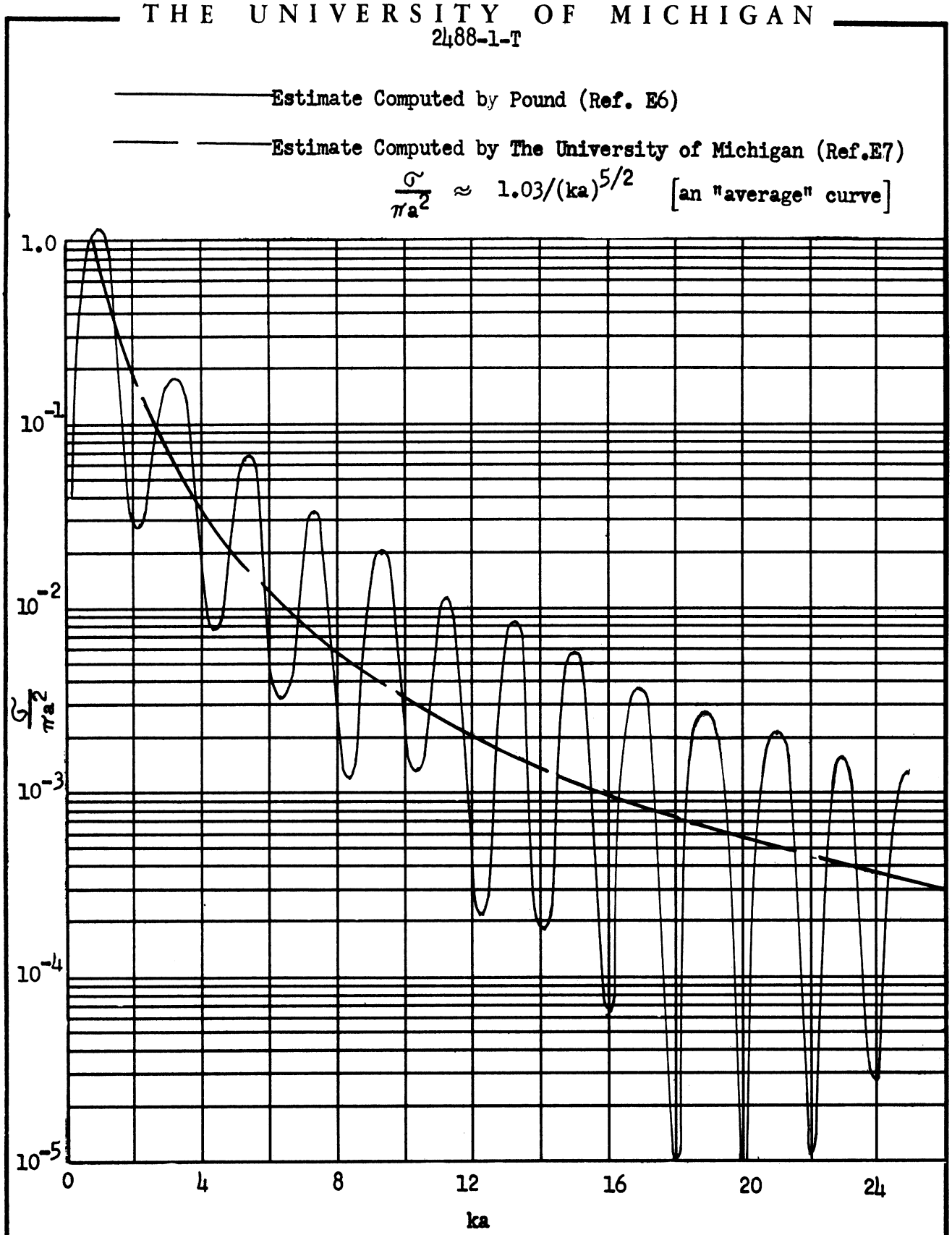

FIG E-2: CONTRIBUTION FROM THE REAR OF A SPHERE OF RADIUS a.

shown in Figure E-2, estimates of the nose-on cross-section of certain thin cones smoothly terminated by spheres or near sphere-like caps are determined in Appendix F and the results so obtained are compared with experiment. In connection with those comparisons between theory and experiment it will be noted from Figure E-2 that over the range of ka involved in the computations, the estimates of Pound deviate from the "average" curve by factors as large as 5 and thus differences of factors of 3 or 4 between theory and experiment are not particularly unexpected. Due to the rapid oscillation of this contribution as a function of ka, it is believed that the "average" curve is more appropriate for the purpose of the comparisons given in Appendix F, since the cap placed upon the cone in these experiments is not truly spherical.

REFERENCES TO APPENDIX E

E1. W. Hansen and L. Schiff, "Theoretical Study of Electromagnetic Waves Scattered from Shaped Metal Surfaces", Stanford University Microwave Laboratory, Quarterly Report No. 3, ATI-104410 (May 1953). UNCLASSIFIED.

E2. C. J. Sletten, "Electromagnetic Scattering from Wedges and Cones", Air Force Cambridge Research Center, Report No. 5090 (July 1952). UNCLASSIFIED.

E3. L. Peters, "Memorandum on the Echo Area of Ogives", The Ohio State University Research Foundation, Report No. 601-7 (January 1956). UNCLASSIFIED.

E4. W. Franz and K. Deppermann, "Theory of Diffraction by a Cylinder as Affected by the Surface Wave", Annalen der Physik, 10, p. 361 (1952).

E5. I. Imai, Z. Phys., 137, p. 31 (1952).

E6. V. E. Pound, Internal Memorandum No. 830-141, Cornell Aeronautical Laboratory, Inc., (18 June 1956). UNCLASSIFIED.

E7. K. M. Siegel, M. L. Barasch, J. W. Crispin, I. V. Schensted, W. C. Orthwein, and H. Weil, "Studies in Radar Cross-Sections XIV - Radar Cross-Section of a Ballistic Missile", The University of Michigan, Engineering Research Institute, Report No. UMM-134 (September 1954). SECRET.

E8. V. A. Fock, Journal of Physics, 10, p. 399 (1946).

APPENDIX F

THE RADAR CROSS-SECTION OF FINITE CONES WITH VARIOUS BASE TERMINATIONS A COMPARISON BETWEEN THEORY AND EXPERIMENT

F.1. Introduction

This appendix gives an account of experimentally determined radar cross-sections of finite cones with various base terminations. Wherever possible, these experimental values are compared with theoretical estimates determined by the methods discussed in the preceding portions of this report. In Section F.2 three finite cones and three cones smoothly capped in the rear ("carrots") are considered. In Section F.3 information on the cross-sections of 7-OC type warheads is presented. In Section F.4 experimental data on other conical shapes is considered. In Section F.5 conclusions are presented.

F.2. The Radar Cross-Section of Carrots and Cones

The Microwave Radiation Company, Inc., performed experimental radar cross-section measurements for the Cornell Aeronautical Laboratory, Inc., on the carrot and cone configurations shown in Figure F-1 (Ref. F1). The results obtained in these experiments are summarized in Figures F-2 through F-4. Estimates of the cross-sections of these configurations have been computed using the techniques discussed previously in this report.

Dimensions (in wavelengths)						
	Carrots			Cones		
	#1	#2	#3	#1	#2	#3
L	2	4	8	2	4	8

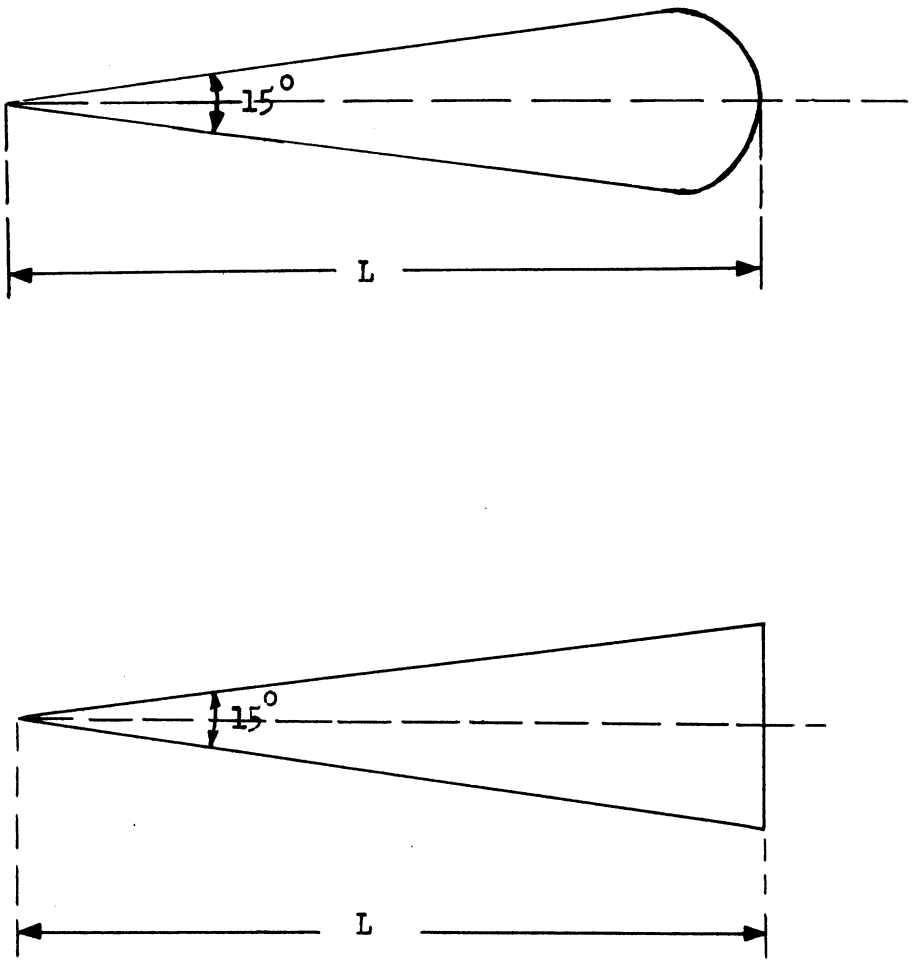

FIG F-1: CARROT AND CONE CONFIGURATIONS

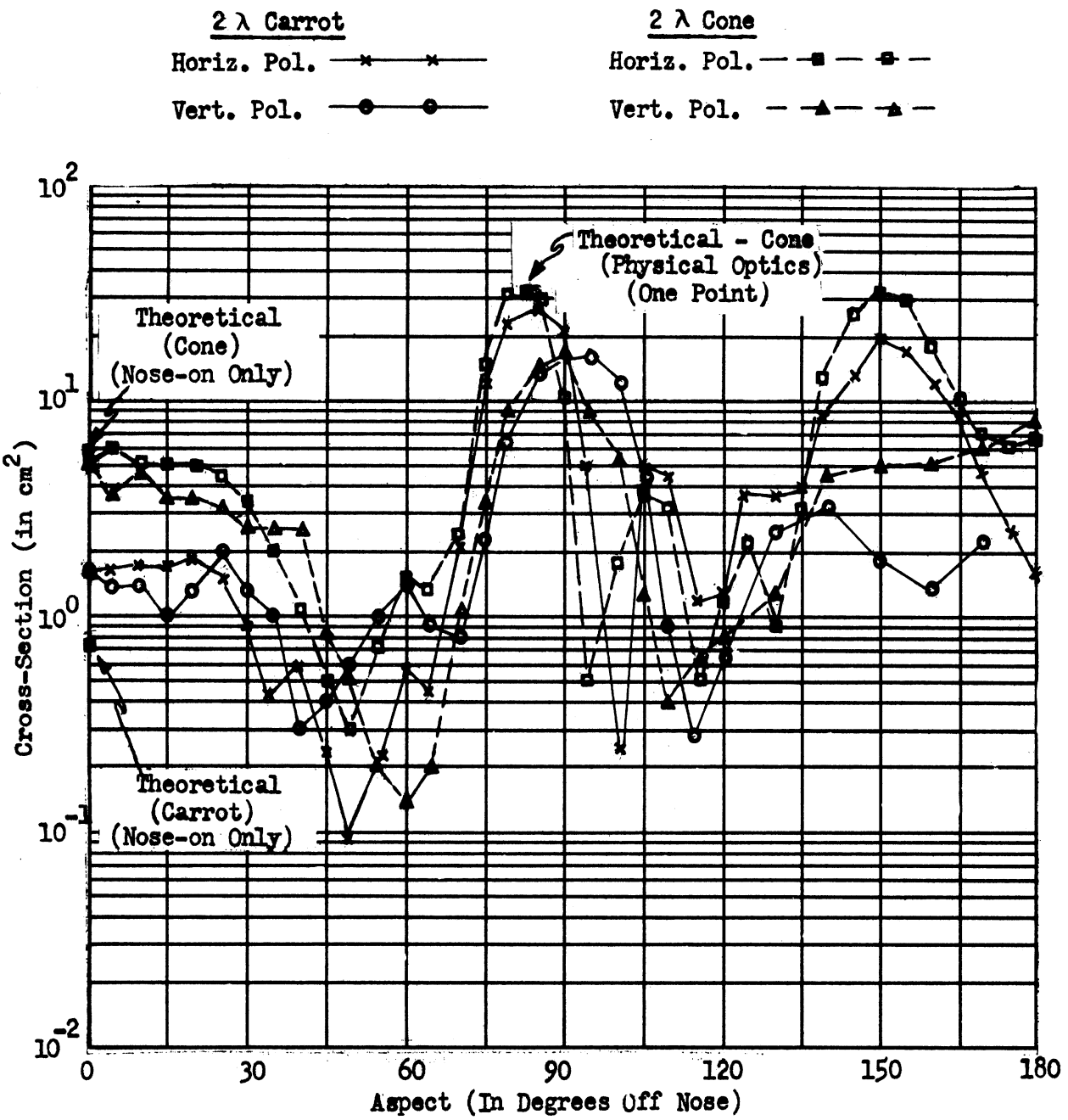

FIG F-2: 2 λ CONE AND 2 λ CARROT - (Ref. F1)
(λ = 3.2 cm)

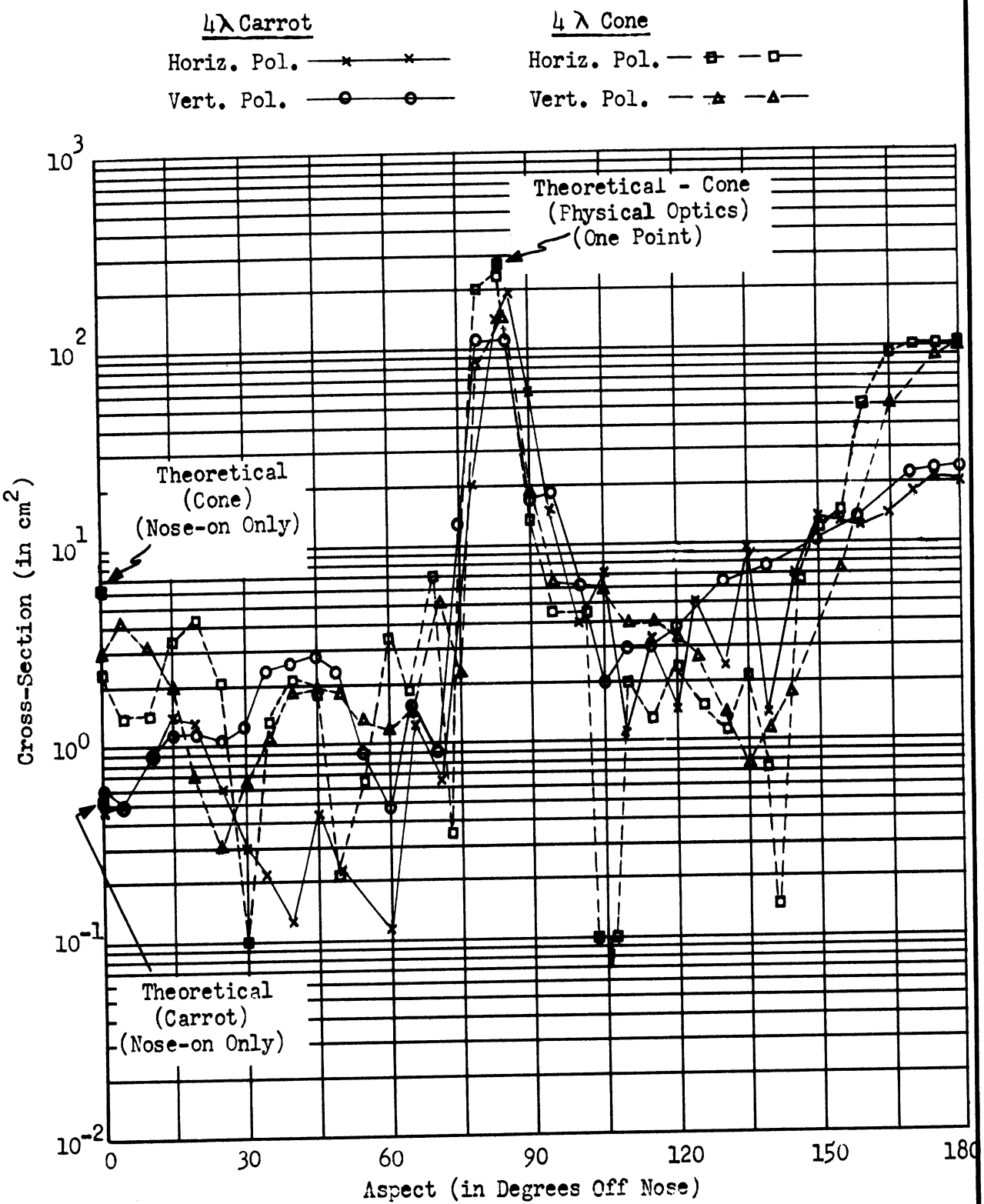

FIG F-3: 4λ CONE AND 4λ CARROT - (REF. F1)
(λ = 3.2 cm)

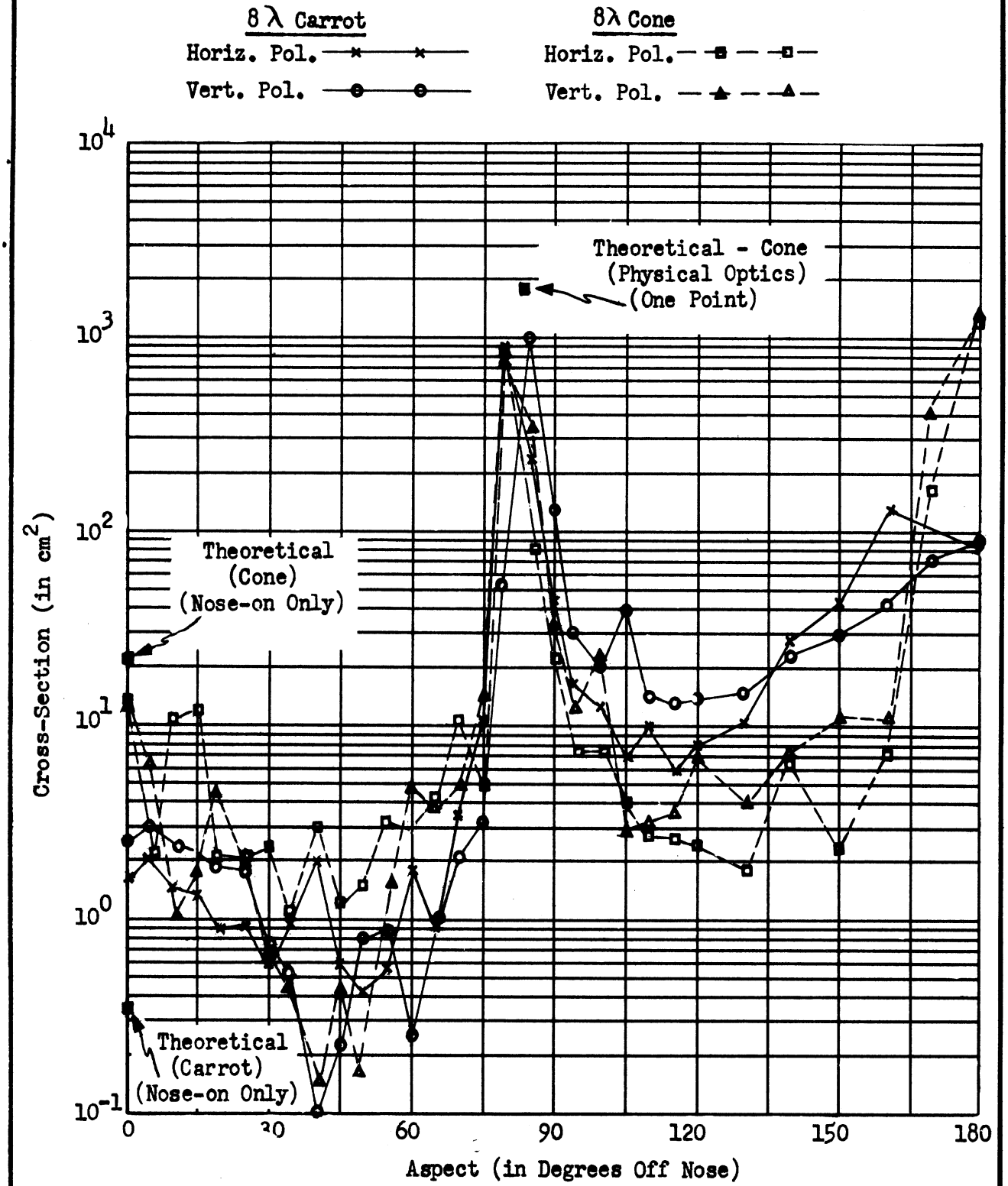

FIG F-4: 8λ CONE AND 8λ CARROT - (REF. F1)
(λ = 3.2 cm)

Theoretical estimates of the nose-on cross-section of the three finite cones are obtained, using the methods described previously in this report for thin cones. That is, an estimate of the graph of cross-section vs a/λ, where a is the radius of the base, is constructed, using the resonant loop answers computed by Kouyoumjian (Ref. F2) faired into the theoretical estimate valid for small wavelengths (i.e., wavelengths for which λ/a is small) developed in Appendix D. The results of these computations are shown in Table F.1 where the nose-on cross-sections of these cones determined theoretically are compared with the experimental data given in Reference F1.

TABLE F.1 - THE NOSE-ON CROSS-SECTIONS OF THE 2λ, 4λ, AND 8λ CONES (λ = 3.2 cm)

BODY	CROSS-SECTIONS (IN CM^2)			
	Exp.Data*	Exp.Data**		Theoretical Estimate***
	Ver.Pol.	Hor.Pol	Ver.Pol.	
2λ cone	3.0	5.3	5.0	5.4
4λ cone	1.1	2.6	3.0	6.5
8λ cone	5.6	13.	17.	23.

*Unpublished data obtained by Professor S. Silver Dept of Electrical Engineering, University of California.

**Reference F1.

***These theoretical values are also shown on Figures F-2 through F-4.

Theoretical estimates of the cross-sections of these cones at an aspect 82.5° off nose have been computed, using the optics formula derived in Reference F3

$$(8\pi L^3 \tan^4\alpha)/(9\lambda \sin^3\alpha)$$

where L is the altitude of the cone and α is the half-cone angle ($\alpha = 7.5°$). The theoretical values so obtained are shown on Figures F-2 through F-4.

It will be noted that the agreement between theory and experiment is excellent at both aspects; this can be seen by reference either to Table F.1 or Figures F-2 through F-4 for the nose-on case and to the figures for the 82.5° aspect.

For the three carrots involved in these experiments the technique described in Appendix E is employed to obtain estimates of the nose-on cross-sections. That is, the cross-section is assumed to be obtained from a contribution from the tip and a contribution which creeps around the rear. The contribution from the rear is estimated by using the theoretical sphere answer in the resonance region with the contribution from the first Fresnel zone removed. This results in the following estimate of the cross-section contribution which creeps around the rear:

$$0.33\,\lambda^2\,(\lambda/a)^{\frac{1}{2}} \quad \text{(Ref.F4)}$$

where a is the radius of the "hemispherical" stern.*

*As pointed out in Appendix E, the appropriate value of a is the radius of curvature at the shadow boundary. However, since this radius of curvature is approximately equal to one-half of the maximum thickness of the body for these carrots and since, as can be seen by reference to Appendix E, we are using an average estimate of this contribution, we can set a equal to one-half the maximum thickness of the body.

The estimates of the nose-on cross-sections of the three carrots obtained in this manner are shown on Figure F-2 through F-4 and in Table F.2. Table F.2, as well as the aforementioned figures, also contains the experimental data from Reference F1.

TABLE F.2 THE NOSE-ON CROSS-SECTION OF THE 2λ, 4λ, AND 8λ CARROTS (λ= 3.2 cm)

Body	Cross-Section (in cm^2)	
	Exp. Data (average of Hor. & Ver. Pol.)	Theoretical Estimate
2λ Carrot	1.7	.72
4λ Carrot	.53	.51
8λ Carrot	2.2	.36

Reference to Table F.2 shows that the agreement between theory and experiment is quite good.

F.3 The Radar Cross-Sections of 7-OC Type Warheads

Experimental data on the 7-OC warhead and modified versions of the 7-OC warhead were reported in Reference F4. These configurations are similar to the carrot and cone shapes discussed above. Sketches of these configurations appear in Figure F-5. Theoretical estimates of the nose-on cross-sections have been determined by the methods described in Section F.2 - the finite cone methods for the 7-OC and the 7-OC with a flat stern, and the formula for determining the contribution which creeps around the rear of the body for the 7-OC with a hemispherical stern. The results so

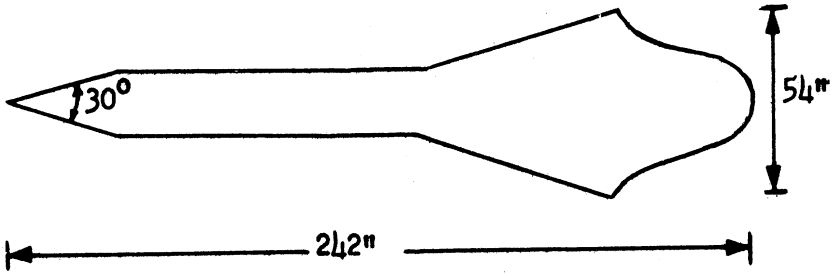

The 7-OC Warhead

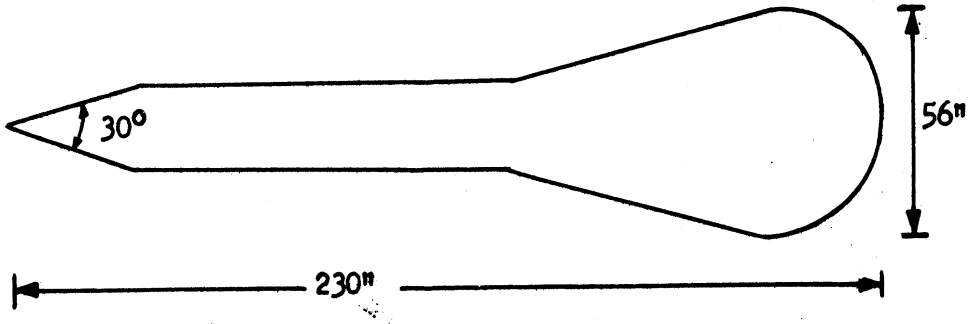

7-OC With a Hemispherical Stern

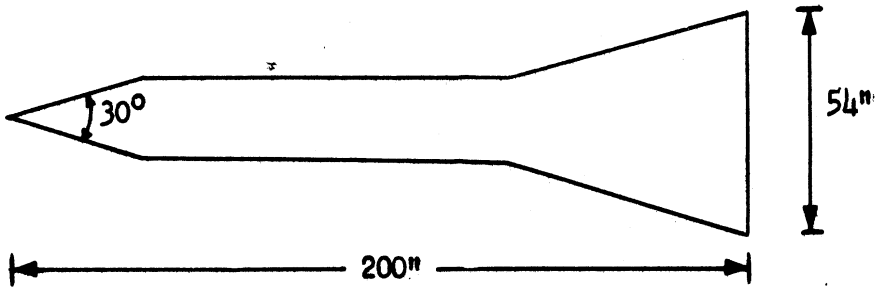

7-OC With a Flat Stern

FIG F-5: 7-OC TYPE MODELS

obtained are given in Table F.3; the experimental data for these configurations is included for comparison purposes. It will be noted that the agreement between theory and experiment is very good.

TABLE F.3 THE NOSE-ON CROSS-SECTIONS OF THE 7-OC TYPE WARHEADS (REFERENCE F4)*

Body	Wave-length (in cm)	Cross-Section (in cm^2)	
		Experiment	Theory
7-OC Warhead	30	12,000 - 15,000	10,000
7-OC Hemispherical Stern	30	60 - 100	140
7-OC Warhead	90	9,000 - 10,000	10,000
7-OC Hemispherical Stern	90	1,500 - 1,600	400
7-OC Warhead	133	4,000 - 9,000	10,000
7-OC Hemispherical Stern	133	250 - 1,800	900
7-OC Flat Stern	133	6,000 - 7,000	10,000

*The experiments are reported in Reference F4; they were performed by The Microwave Radiation Company, Inc., and by the Evans Signal Laboratory.

F.4 Other Experimental Data on Cones

F.4.1 Data From the Federal Telecommunications Laboratories, Inc.

W. Sichak in Reference F5 has reported the results of experiments conducted on three thin finite cones; these cones have half-cone angles of 5.1° and 9.6°. Sichak's data, together with the theoretical estimates obtained by the procedure described in Section F.2, are presented in Table F.4.

TABLE F.4 NOSE-ON CROSS-SECTIONS OF FINITE CONES
USED IN FEDERAL TELECOMMUNICATIONS LABORATORIES EXPERIMENTS

Half-Cone Angle (in degrees)	Altitude of Cone (in cm)	Wavelength (in cm)	Cross-Section (in cm^2)	
			Experiment	Theory
9.6	15.25	1.25	4	13
5.1	15.25	1.25	0.6	3.6
9.6	7.63	1.25	0.9	3.4

F.4.2 Data From the Belmont Radio Corporation

The data from the Belmont Radio Corporation (Ref. F6) were obtained from an experiment conducted on a thin cone having a half-angle of $\sim 10^{\circ}$. The experiment was conducted at a wavelength of 1.26 cm and the radius of the base of the cone was equal to 0.59λ. The experimental value of the nose-on cross-section of this cone is 0.87 cm^2. Applying the techniques previously described in this Appendix, a theoretical estimate of 1.1 cm^2 is obtained.

F.4.3 British Experiments on Cones Capped With Cylinders

On a recent trip to England the author was informed by J. S. Hey of the Radar Research Establishment of recent British experiments on cones faired into cylinders. From these experiments, which were conducted on four different cones capped with cylinders of varying length, average values were obtained. These values, together with theoretical estimates, are given in Table F.5. The theoretical estimates were obtained by using the expression derived in Appendix D (Equation 6 of Appendix D).

TABLE F.5 NOSE-ON CROSS-SECTIONS OF FINITE CONES FAIRED INTO CYLINDERS (UNPUBLISHED BRITISH EXPERIMENTAL DATA AND THEORETICAL ESTIMATES)

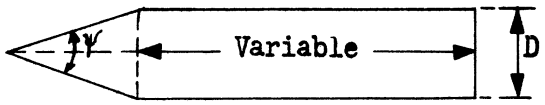

D (in λ)	$\psi/2$	Cross-Section (in λ^2)	
		Experimental Average	Theoretical Estimate
1.8	10°	0.2	0.08
1.8	30°	0.3	0.4
3.0	10°	0.3	0.2
3.0	30°	0.5	1.0

F.4.4 Experimental Data on Thick Cones With Smoothly Rounded Bases

The work of C. J. Sletten (Ref. F7) has indicated that if the cone angle is not too small and if $ka >> 1$, then the nose-on cross-section of a smoothly rounded cone is adequately predicted by the physical optics formula, $\lambda^2 \tan^4\theta/16\pi$, where θ is the half-cone angle. Sletten's experimental data are compared with this physical optics expression in Figure F-6.

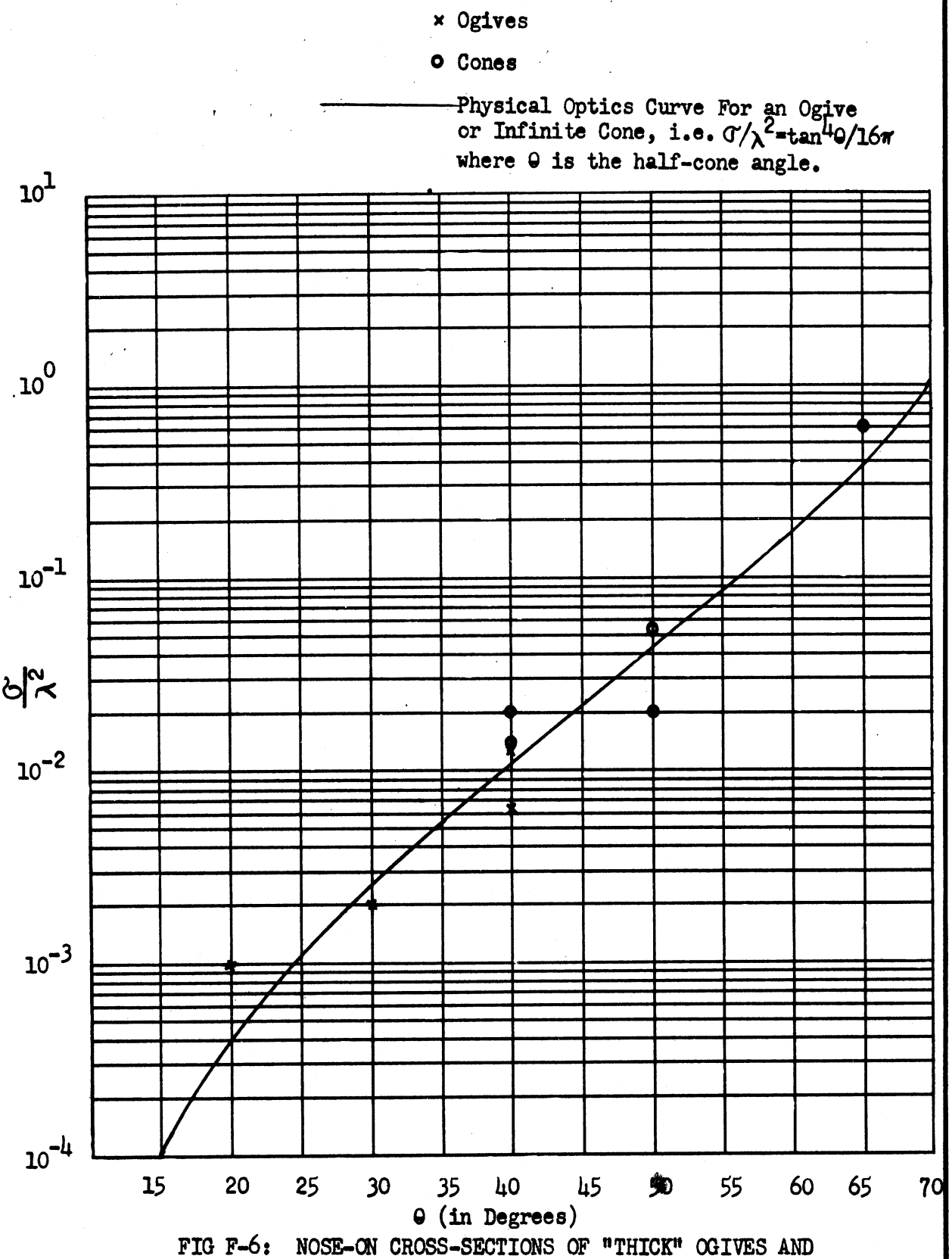

FIG F-6: NOSE-ON CROSS-SECTIONS OF "THICK" OGIVES AND SMOOTHLY ROUNDED CONES (REF. F7)

F.5 Conclusions

It has been observed in this appendix that the techniques employed to obtain theoretical estimates of the nose-on cross-sections of finite cones and finite cones which are smoothly terminated are in good agreement with experimentally determined values.

In addition it has been noted that there is, in general, at most one order of magnitude difference between the cross-sections of thin finite cones, smoothly rounded or not, if the over-all length of the configuration ranges from 2 to 8 wavelengths, especially for aspects out to 60° off nose. This is illustrated in Figure F-7. Thus, it is seen from the experimental data that if the radius of the base is comparable to the wavelength, the nose-on cross-section of the "carrot" is comparable to the nose-on cross-section of the comparable cone. If, on the other hand, the wavelength is small in comparison to this base-radius, the two nose-on cross-sections are considerably different. This trend can be seen from the material presented in Section F.4.

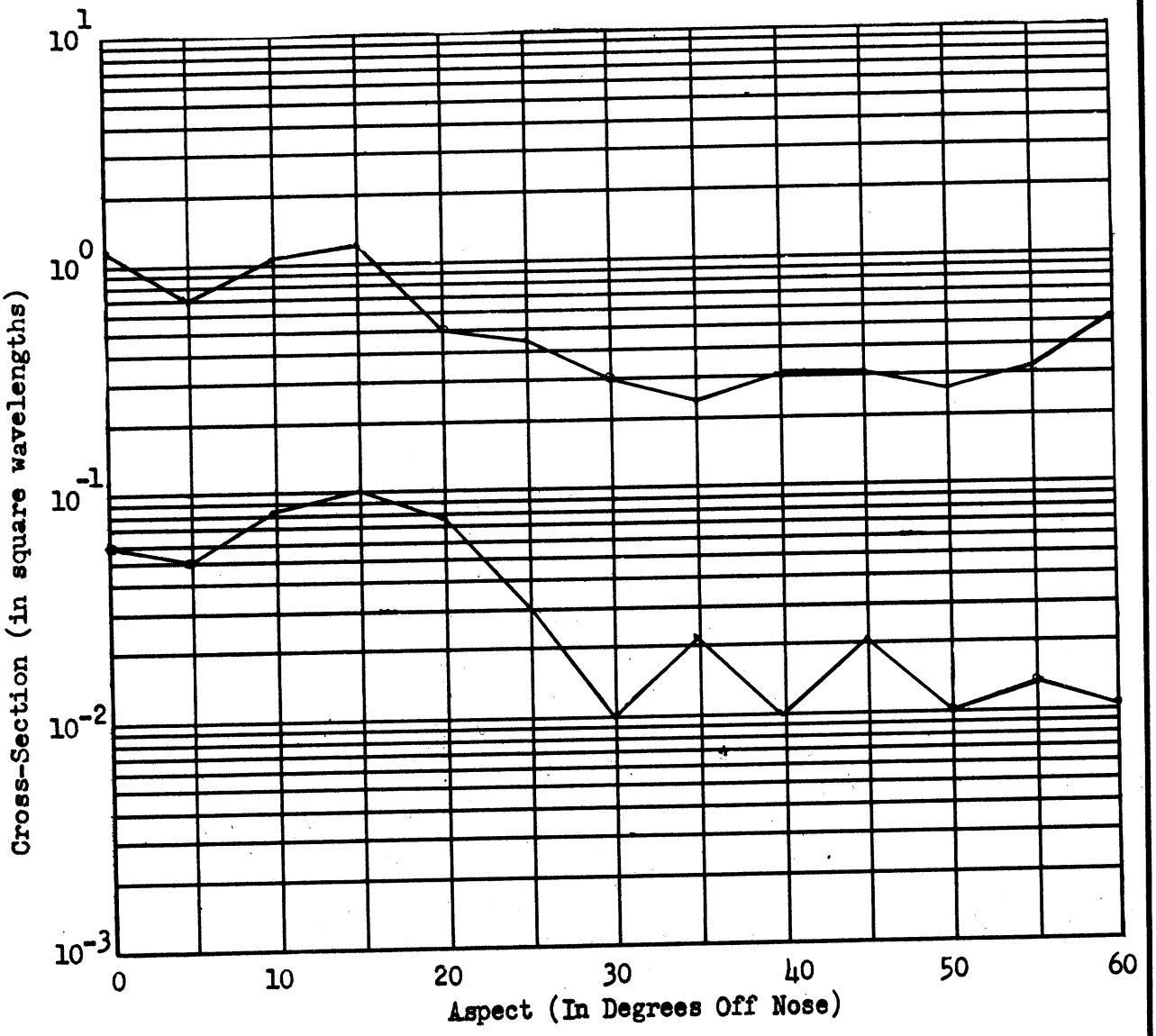

FIG F-7: LIMITS ON EXPERIMENTAL DATA FOR 7.5° CARROTS AND CONES
(Horizontal and Vertical Polarizations)

REFERENCES TO APPENDIX F

F1 - "Radar Back Scattering Cross-Sections of Three Configurations," Microwave Radiation Company, Inc., Report No. 203, (Work Performed for the Cornell Aeronautical Laboratory, Inc. under Contract DA-30-115-ORD-543), July 1955. SECRET.

F2 - R. G. Kouyoumjian, "The Back Scattering From a Circular Loop," The Ohio State University Research Foundation, Report 662-5, April 1956. UNCLASSIFIED.

F3 - C. E. Schensted, J. W. Crispin, and K. M. Siegel, "Studies in Radar Cross-Sections XV - Radar Cross-Sections of B-47 and B-52 Aircraft," The University of Michigan, Engineering Research Institute, Report 2260-1-T, August 1954. CONFIDENTIAL.

F4 - K. M. Siegel, M. L. Barasch, J. W. Crispin, I. V. Schensted, W. C. Orthwein, and H. Weil, "Studies in Radar Cross-Sections XIV -- Radar Cross-Section of a Ballistic Missile," The University of Michigan, Engineering Research Institute, Report UMM-134, September 1954. SECRET.

F5 - W. Sichak, "Missile Detection - Final Report," Federal Telecommunications Laboratories, Inc. Contract W 36-039-sc-32119, ATI 42811 (August 1948). SECRET.

F6 - "Research Investigations on Counter-Battery and Fire Control Radar," Belmont Radio Corporation, Final Report, (May 1948). SECRET.

F7 - C. J. Sletten, "Electromagnetic Scattering From Wedges and Cones," Air Force Cambridge Research Center, Report No. 5090, (July 1952). UNCLASSIFIED.